RESEARCH ARTICLE   OPEN ACCESS

Structural Control on the Complex Platform to Basin Transition of a Mississippian Carbonate Platform in the Southern East Irish Sea Basin, UK

Maulana Rizki Aditama[1,2] 🟢 | Mads Huuse[1] | David Healy[3] | Darren Jones[4,5] | Cathy Hollis[1] 🟢

[1]Department of Earth and Environment, The University of Manchester, Manchester, UK | [2]Geological Engineering Department, Universitas Jenderal Soedirman, Purwokerto, Indonesia | [3]Geosolutions, School of Earth and Environment, The University of Leeds, Leeds, UK | [4]British Geological Survey, Edinburgh, UK | [5]Geoscience and Technology Department, TNO, Utrecht, the Netherlands

Correspondence: Maulana Rizki Aditama (maulana.aditama@manchester.ac.uk; maulanarizkia@unsoed.ac.id)

ABSTRACT

Mississippian-aged (Lower Carboniferous) syn-rift carbonate platforms in the UK have been extensively studied in outcrop. They have been interpreted to grow principally on the footwall of faults, with deeper marine sedimentation in the adjacent hanging wall basins. However, the transition from the shelf margin to the basin is often poorly constrained due to a lack of exposure and the scarcity of high-quality seismic data. With renewed interest in Mississippian carbonate strata as potential geothermal reservoirs in northern Europe, a better understanding of the detailed geometry of these carbonate platforms, and the controls on their growth and demise, is crucial as it provides insights into their occurrence, size and thickness and burial/exposure history. This study uses high-resolution 3D seismic data from the southern part of the offshore East Irish Sea Basin (EISB), western UK, to identify, characterise and map the platform to basin transition of the North Wales carbonate platform, exposed on the North Wales coastline. The results indicate that there is not a simple platform to basin transition, as has previously been mapped, but that the North Wales platform gives way offshore to numerous small carbonate platforms, the presence of which is predominantly controlled by N-S-oriented extensional faults. The fault orientation is not consistent with the regionally interpreted N-S stress direction during the Mississippian, but fault growth analysis suggests that their orientation most likely reflects the precursor structural grain. These faults facilitated the development of horst-graben structures, promoting carbonate growth on footwalls within the EISB. Six areas of potential carbonate platform development (A1–A6) were mapped and evaluated. Thicknesses range from ~1 to 2 km. The platforms prograded during the Tournaisian, characterised by low-angle slopes, followed by a backstepping phase in the Visean, marked by steeper slopes. The platforms significantly shrank in size from the early Tournaisian to the Visean, resulting in the formation of complex, patchy carbonate platforms with diverse shapes and sizes. The results demonstrate that numerous small carbonate platforms grew in the EISB on structural highs but were susceptible to environmental change at the end of the Mississippian, causing them to become increasingly isolated and to eventually drown.

Summary

- Mississippian carbonate platforms (MCPs) exhibit complex, fault-controlled architectures rather than a simple platform-to-basin transition, resulting in irregular shapes and patchy distributions.
- Depth-converted maps of the MCP top reveal steep-slope platform geometries with fault-controlled margins.
- Platform margin angles were lower during the early Mississippian (initiation phase), while the late Mississippian stage was marked by platform steepening, backstepping and significant size shrinking.
- Six distinct carbonate platform types within the hanging wall basin exhibit variations in thickness and geometry, primarily influenced by fault activity and subsidence.

1 | Introduction

This study uses conventional 3D seismic reflection data, originally acquired to image shallower Permian–Mesozoic strata, to identify and characterize Lower Carboniferous (Mississippian-aged) carbonate strata. It focuses on the East Irish Sea Basin (EISB), UK (Figure 1a) since it is directly offshore of the well-exposed North Wales carbonate platform. The margin of this platform has previously been interpreted to form a linear feature immediately offshore of the North Wales coastline (Pharaoh, Kirk, et al. 2016; Pharaoh et al. 2018; Kirkham 2021; Manifold et al. 2021). Specifically, the study aims to describe the offshore transition of the North Wales Platform into the EISB and determine whether fault activity influenced carbonate platform architecture. On this basis, a secondary aim was to assess the evidence for a structural control on platform growth and demise.

This study is timely because of a renewed interest in Mississippian carbonate strata as potential low-enthalpy geothermal reservoirs. Mississippian carbonate platforms lie at favourable burial depths and temperatures beneath major UK population centres, making them strategic targets for geothermal heat generation (Bos and Laenen 2017; Mijnlieff 2020; Pharaoh et al. 2021; Jones et al. 2023). Although geothermal exploitation of age-equivalent carbonate strata is underway in northern Europe (Broothaers et al. 2021), the UK context is complicated by variability in platform thickness and the limited resolution and penetration of onshore geophysical data. Borehole records show Mississippian carbonate units ranging in thickness from ~150 m to over 3600 m across NW England, one key area for exploration (Greater Manchester, Cheshire, Lancashire and South Cumbria; Jones et al. 2023), but the absence of wells intersecting the top Mississippian carbonate strata, and the limited penetration of the basal units in many areas, constrain understanding of the controls on stratal thickness, the complexity of platform geometries and architecture and consequently their viability as geothermal targets.

Mississippian carbonate platforms onshore in the UK have been extensively studied in outcrop and are widely interpreted to have grown on the footwalls of normal faults (Ebdon et al. 1990; Fraser et al. 1990; Fraser and Gawthorpe 2003). At a regional scale, their occurrence is interpreted to be controlled by major structures formed by pre- to post- Palaeozoic tectonic events (Figure 1c; Fraser et al. 1990; Fraser and Gawthorpe 2003). Conceptual models assume a relatively simple facies transition from platform carbonates developed on the footwalls of basement-involved normal faults during back-arc extension, to hanging wall basins dominated by remobilised carbonate and pelagic siliciclastic sediments (Fraser and Gawthorpe 2003). Platform distribution and architecture in the subsurface; however, remain poorly constrained, not least because of the sparse distribution and poor quality of 2D seismic lines onshore UK. This project addresses this issue by using 3D seismic reflection data from the EISB, offshore UK. By focusing on the southern part of the EISB, it is possible to interpret the seismic data in more detail than onshore data allow and integrate outcrop data collected on the North Wales coastline (Juerges et al. 2016; Kirkham 2021; Manifold et al. 2020, 2021; Figure 1b). Previous studies using EISB seismic data have typically focused on the regional-scale structural framework and post-Carboniferous fill (Figure 1a,c) (Pharaoh et al. 2018, 2020), without detailed analysis of Mississippian stratal architecture. This study builds on that work at the sub-basin scale by conducting a detailed fault analysis and evaluating carbonate platform architecture in more detail, incorporating seismic facies analysis.

2 | Geological Setting

2.1 | Regional Geology

The EISB is part of a broader region encompassing offshore northern England, north Wales and southern Scotland. It has undergone multiple phases of tectonic deformation (Jackson and Mulholland 1993; Phillips et al. 2017) with its geological evolution shaped by the interplay of large-scale extensional and compressional events associated with the closure of the Rheic Ocean and the subsequent Variscan Orogeny (Corfield et al. 1996), followed by Mesozoic extension and Alpine inversion (Fraser and Gawthorpe 2003). Following the Caledonian Orogeny, a phase of post-orogenic relaxation occurred during the Late Devonian. This led to the gravitational collapse of the previously thickened crust and the initiation of extensional tectonics (Chadwick et al. 1993; Smit et al. 2018). Normal faulting became widespread, driving the early development of rift basins across Avalonia (Chadwick et al. 1993; Quirk and Kimbell 1997; Smit et al. 2018). The onset of this extensional regime marked the beginning of a long-lived tectonic cycle, culminating in the Variscan Orogeny, the effects of which were felt in the region during the late Carboniferous (Gamboa et al. 2019; Knipe et al. 1993; Underhill and Richardson 2022; Yaliz and Chapman 2003).

During the Tournaisian, northern England was dominated by a regional extensional-transtensional tectonic regime, with the main stress direction oriented north-south (N-S) to northwest-southeast (NW-SE) (Figure 2; Fraser and Gawthorpe 2003; Coward 1993, 1995). More specifically, dextral transtensional tectonics with a clockwise rotational component resulted in NE–SW-directed extensional reactivation of east to northeast-trending Caledonian basement structures (Smit et al. 2018). There was also a shift in the structural polarity of the basin at this time, leading
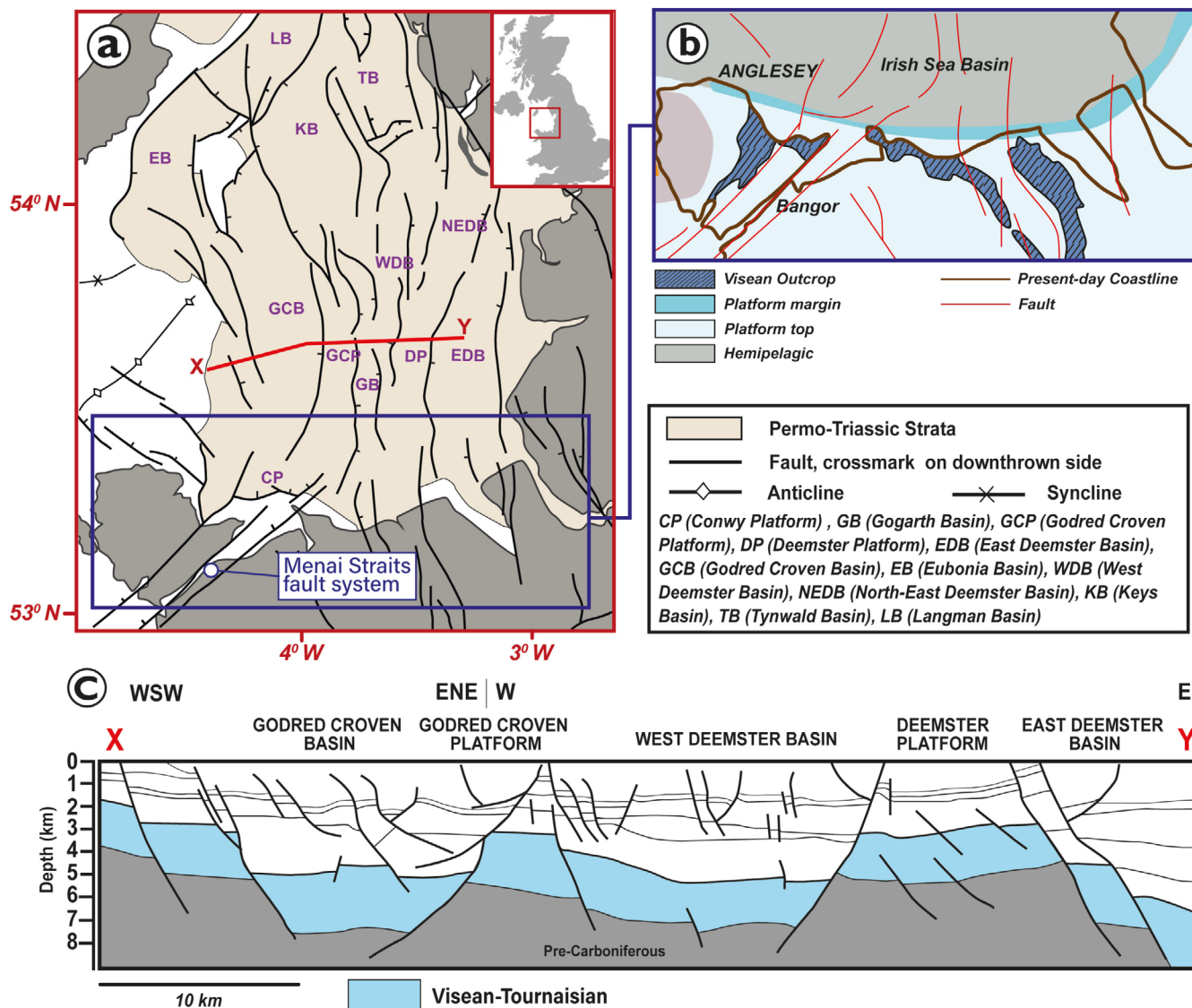
FIGURE 1 | (a) Simplified geological map of the East Irish Sea Basin (EISB), highlighting Permo–Triassic strata and major structural elements, along with basin and platform names (modified from Jackson et al. 1995). (b) Detailed geological map of the North Wales Platform and its surrounding area in the Irish Sea Basin, illustrating the distribution of the Mississippian carbonate. Key structural features, including platform margins, platform tops, hemipelagic zones, Palaeozoic basement, faults and present-day coastlines, are mapped and showing the position of the interpreted Visean carbonate platform prior to this study (modified from Manifold et al. 2021; Ebdon et al. 1990; Fraser and Gawthorpe 1990, 2003; Pharaoh et al. 2018). (c) Representative WSW–E cross-section across the central East Irish Sea, illustrating regional-scale horst and graben geometry, with a particular focus on the deeper-level occurrence of the Carboniferous Limestone Supergroup (modified from Jackson et al. 1995).

to subsidence along the southern margin of the basin (Corfield et al. 1996; Smit et al. 2018). The EISB is bounded by the North Wales Platform to the south, the Lake District Block to the northeast and the Solway Basin to the north, with its southern sector forming the focus of this study. It has been described by Fraser and Gawthorpe (2003) as a hanging-wall basin relative to the NWP, but the structural boundary is not defined by a single E–W extensional fault. Instead, the basin architecture is influenced by a complex network of faults, predominantly trending N–S to NW–SE, including the long-lived Menai Strait Fault System (MSFS; Figure 1), which has accommodated significant deformation across multiple tectonic phases (Schofield et al. 2021).

The tectonostratigraphic evolution of the northern UK during the Carboniferous can be broadly divided into syn-rift, post-rift

and inversion megasequences (Fraser and Gawthorpe 2003; de Jonge-Anderson and Underhill 2020; Jackson et al. 2011). The syn-rift megasequence, marked by extensional tectonics and fault-controlled sedimentation, spanned the late Devonian and Mississippian, terminating in the Serpukhovian (Figure 2) (Fraser and Gawthorpe 2003; Manifold et al. 2021; Somerville 2008; Somerville et al. 1989). This broadly coincided with the onset of the Gondwana glaciation, continental reorganisation and the closure of the Rheic Ocean. The sub-equatorial location of the Pennine and Irish Sea Basins during the Mississippian enabled prolific carbonate production and platform development in the region's shallow-water environments (Corfield et al. 1996; Wright and Vanstone 2001; Somerville 2003; Manifold et al. 2021). Significant variations in carbonate platform thickness and facies have been described
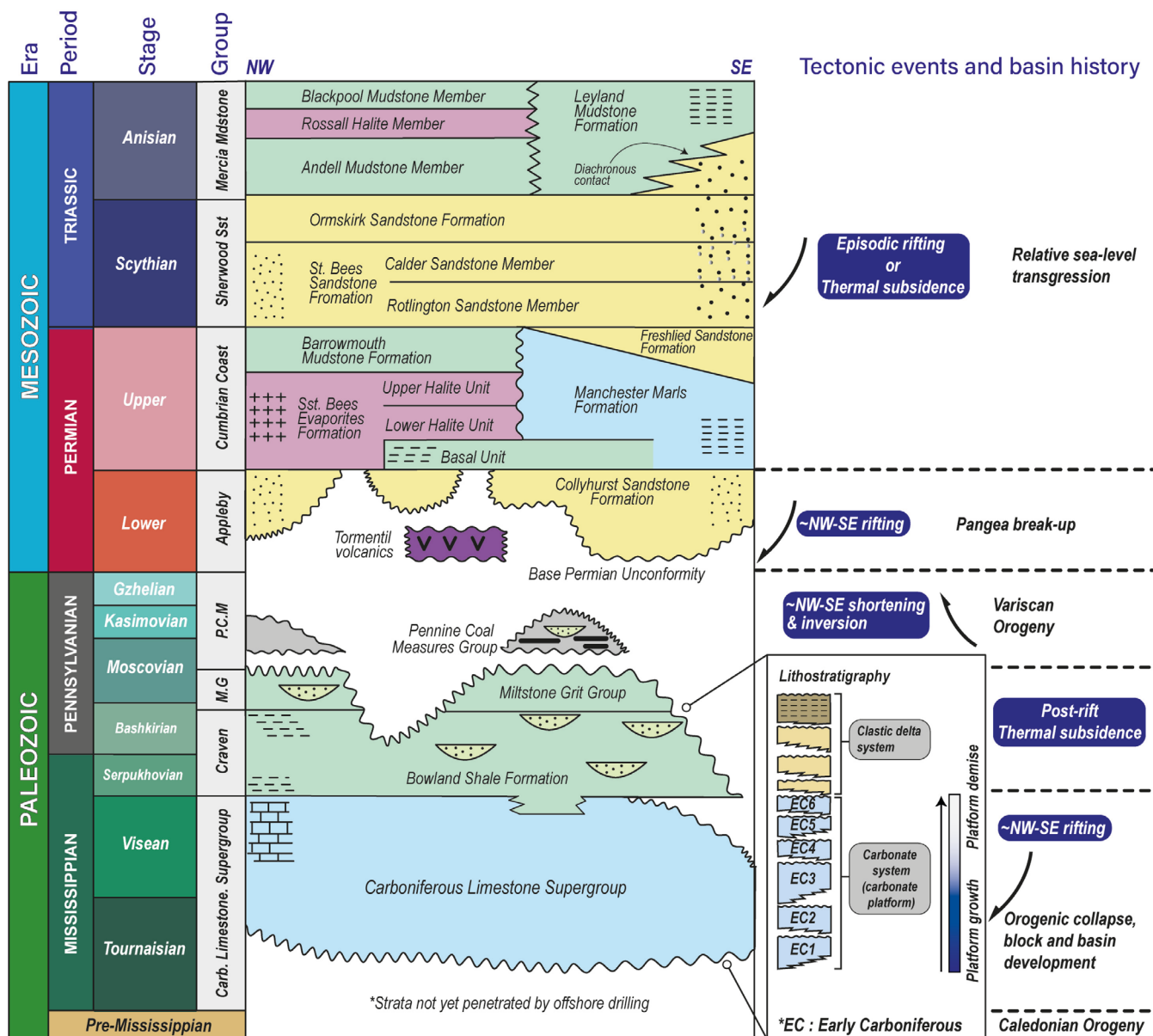
FIGURE 2 | A generalised stratigraphic column spanning from the Pre-Mississippian to the Triassic is presented, illustrating the eras, periods, stages, groups, tectonic events and basin history. Beginning with the Pre-Mississippian, the Lower Carboniferous (Mississippian), composed of sequences EC1–EC6, is shown to develop within a complex rifting tectonic environment, where carbonate growth and eventual demise occurred during the Tournaisian to Visean stages. Note that the youngest Mississippian carbonate strata are now interpreted to be Serpukhovian in age (Lucas et al. 2022). Adapted from Fraser and Gawthorpe (2003) and Jackson et al. (1997).

across major normal fault zones bounding half-graben depocenters onshore (Adams et al. 1990; Fraser and Gawthorpe 2003; Somerville 2005).

Post-rift sedimentation (Bashkirian–Moscovian) was characterised by the deposition of turbidite-fronted fluvio-deltaic sediments that infilled the basin during thermally driven subsidence (Fraser and Gawthorpe 2003). These deposits extend across both the eastern and western margins of the EISB, linking with correlative post-rift successions documented offshore and onshore in Ireland. Finally, the Variscan Orogeny led to the formation of the inversion megasequence (Moscovian–Permian), a period of compression associated with the closure of the Rheic Ocean to the south, widespread fault reactivation

and regional uplift affecting the entire Irish Sea domain (Chadwick and Evans 1995; Fraser and Gawthorpe 1990, 2003; Smit et al. 2018).

2.2 | Mississippian Carbonate Sedimentology

During the Mississippian (358.9–330.9 Ma; Lucas et al. 2022), Britain was situated at sub-equatorial latitude, which facilitated the deposition of carbonates in a warm, shallow shelf sea to the north and south of the Wales-Belgium Massif (Davies 2008; Pharaoh et al. 2021; Smit et al. 2018). These carbonate deposits were extensive, deposited on land-attached and isolated carbonate platforms (Wright and Vanstone 2001;

Fraser and Gawthorpe 2003; Davies 2008). Mississippian carbonate strata were classified into six tectono-stratigraphic megasequences (EC-1–EC-6) by Fraser and Gawthorpe (2003) (Figure 2).

Carbonate sedimentation began across Europe in the Tournaisian (Wright 1980) and by the Visean, extensional tectonics played a crucial role in the development of shallow marine carbonate platforms on footwall highs across northern England (Ebdon et al. 1990; Fraser et al. 1990; Pickard et al. 1994; Fraser and Gawthorpe 2003). These were primarily photozoan platforms, dominated by warm, clear-water carbonate production, where light availability and low siliciclastic input favored the growth of skeletal and microbial carbonate facies (Wright 1980; Wright and Vanstone 2001; Somerville 2005; Manifold et al. 2021). By the mid-Visean, fault-controlled subsidence and carbonate productivity had enhanced the topographic contrast between the shallow-water carbonate platforms on footwalls and the adjacent hanging-wall basins, steepening the platform margins, facilitated by cementation of slope margins (Schofield and Adams 1985; Della Porta et al. 2004; Manifold et al. 2021). The North Wales Platform grew as a land-attached carbonate platform covering approximately 1200 km^2 on the southern margins of the Irish Sea Basin (Juerges et al. 2016; del Strother et al. 2021; Manifold et al. 2021) and the carbonate platform described in this study is the offshore extension of this platform.

3 | Data and Methods

3.1 | Dataset

This study utilises multiple 3D seismic datasets covering the southern EISB and adjacent areas (Figure 3, Table 1). The seismic volumes vary in vintage, resolution and spatial coverage. Most were acquired in the 1990s and processed using post-stack time migration (PSTM), with no pre-stack depth migration or velocity model applied. The data are post-stack time migrated with a bin spacing of 12.5×12.5 m and a sampling interval of 4 ms. All volumes are zero-phased, following SEG normal polarity, where a positive reflection coefficient indicating an increase in acoustic impedance is shown as a red peak, while a negative reflection coefficient (a decrease in impedance) is shown as a blue trough. Acquisition was undertaken in a shallow-water bathymetric setting (50–75 m depth). Frequency characteristics and acquisition details are summarised in Table 1. As these datasets were primarily designed to image shallower, Permo-Triassic targets, they are not optimised for deep imaging of Mississippian carbonate strata. Vertical resolution across the study area ranges between 25 and 62.5 m, depending on the seismic vintage and processing parameters (Table 1). Medium- to high-resolution data (25–29 m) are associated with more recent 3D volumes over the Deemster Platform (Hamilton Field), North Wales Offshore and parts of the Solway Basin, allowing for improved imaging of platform geometries and reflector continuity. In contrast, lower-resolution data (48–62.5 m), such as those covering the West Deemster Basin, are based on older vintages with more limited frequency content and reduced interpretability at depth. The frequency content of several datasets declines significantly below ~2s TWT, further reducing vertical resolution within the deeper Mississippian interval. Given the combination of variable seismic data quality and large spatial coverage, these differences in resolution introduce interpretational uncertainty, particularly when comparing platform morphologies across the basin. Interpretation was therefore conducted with an awareness of these limitations, with more caution applied in areas where imaging was constrained by lower-resolution legacy data.

Well control within the study area was limited. Data from well 110/08-1 was available, but its penetration only extended into the Serpukhovian (Figure 4). The nearest wells that reach the top Mississippian strata (e.g., 111/25-1A, 112/25a-1, 112/15-1, Silloth-1A) are located approximately 50–100 km to the north, within the Solway Basin and adjacent areas (Figure 3). These offset wells, along with prior seismic mapping, were used to inform horizon interpretation in the study area (Pharaoh, Smith, et al. 2016; Pharaoh et al. 2018; Stuart and Cowan 1991). These surfaces were then quality controlled, revealing that the existing surfaces did not consistently adhere to a specific reflector. To ensure consistency, refinement or repicking was performed along individual reflections, as the low resolution of previous regional studies based on 2D seismic data and heavily interpolated often resulted in surfaces crossing multiple reflections in the 3D seismic data.

3.2 | Methods

3.2.1 | Depth Conversion and Generation of Structure Maps

The depth conversion of seismic surfaces was conducted to generate depth-structure maps. A time-depth curve approach was applied to achieve an optimal fit while accounting for associated uncertainties (Couleou 2020; Deraisme and Jeannee 2020). This process was challenged by the limited availability of well data penetrating Mississippian strata and the scarcity of velocity data. To mitigate these challenges and reduce uncertainties, the depth conversion approaches were tested to determine the most reliable method.

The primary approach utilised two-way travel time (TWT) versus depth data derived from checkshot surveys from four key wells (110/11-1, 110/08-1, 110/12-B4 and 110/11a-3, Figure 4). This approach was adopted from a similar study on seismic depth conversion, that used localised velocity information to refine the overall model (Armstrong et al. 2004; Pharaoh, Kirk, et al. 2016; Reijmer et al. 2017). The checkshot data from these wells were plotted against depth, revealing a consistent velocity trend across all wells despite varying depths of penetration. Well 110/08-1, drilled within the Deemster platform area, reached a maximum depth of approximately 1.5 km, terminating within the Millstone Grit Group (Figure 4). In contrast, well 110/11-1, located in the Gogarth Basin, penetrated to approximately 3.5 km, also encountering the Millstone Grit Group. Since none of the wells fully penetrated the Mississippian, a polynomial regression equation was derived, where y represents depth (m) and × represents TWT (ms) (Table 2).

A key feature of carbonate platforms, and their offshore transition, is their slope angle, since most classifications of carbonate platform morphology are based upon carbonate slope angle. To evaluate the impact of uncertainties in time-depth conversion
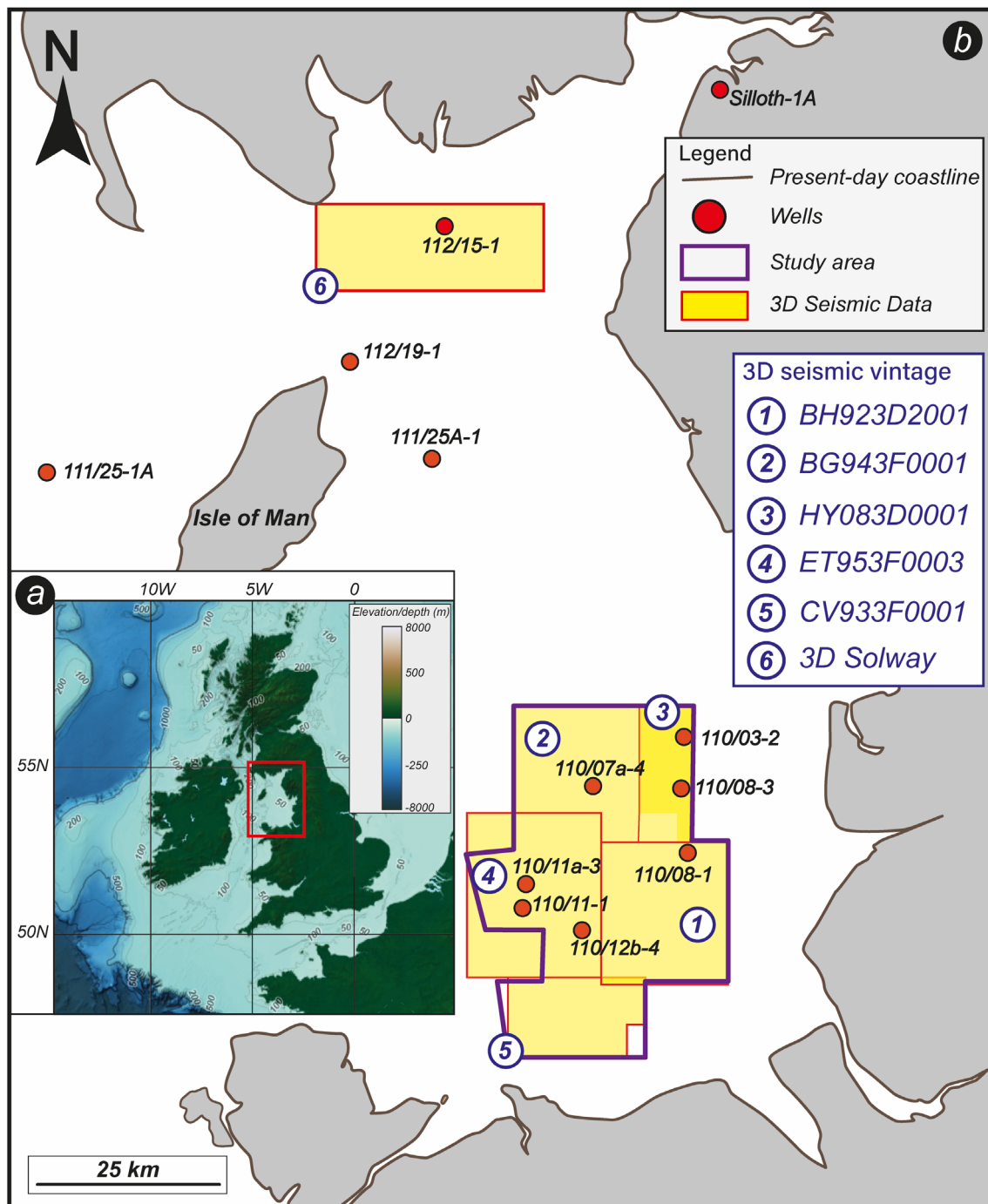
FIGURE 3 | Overview of datasets used in this study. (a) Bathymetry map of the Irish Sea and adjacent areas, derived from EMODnet data (EMODnet Bathymetry Consortium 2022). (b) Spatial distribution of 3D seismic surveys (outlined in yellow boxes and labelled numerically) and well data locations (marked by red circles) incorporated into the analysis.

on stratal dip, particularly platform slope and fault angle interpretations, three polynomial regression models were tested (Figure 4):

1. Combined well: Incorporating data from all four wells, yielding the equation: $y = 0.0003x^2 + 1.6516x - 57.912$

2. Single Well based solely on data from the deepest well, 110/11-1, resulting in the equation: $y = 0.0002x^2 + 1.9382x - 157.07$

3. Single well taken from the shallow penetration, 110/08-1, resulting in the equation: $y = 0.0008x^2 + 1.1721x + 18.372$

To quantify depth estimation differences, 100 ms TWT error bars were incorporated and applied at 1800 ms TWT. Assuming that, the slope of platform margins was estimated at a 1 km horizontal distance, allowing for the calculation of slope angle changes. The TWT vs. depth plots indicate that all models exhibit similar trends at shallower depths, with slight deviations at ~2 km and increasingly large differences at depths exceeding 3 km (Figure 4). The greater discrepancies at depth are attributed to the fact that shallow wells rely primarily on extrapolated velocity trends, as their checkshot data extend only to 1 km depth and therefore error increases with depth.

TABLE 1 | Summary of available 3D seismic reflection data (time domain) and well exploration information used in the Irish Sea Basin and adjacent areas. The table includes the depth to the deepest interpreted marker and the associated interpreter or data source reference. Although the Solway Basin and its surrounding regions are not part of the analysis, they are included for spatial comparison to illustrate the proximity to key wells that penetrate the Mississippian (Carboniferous Limestone Supergroup).

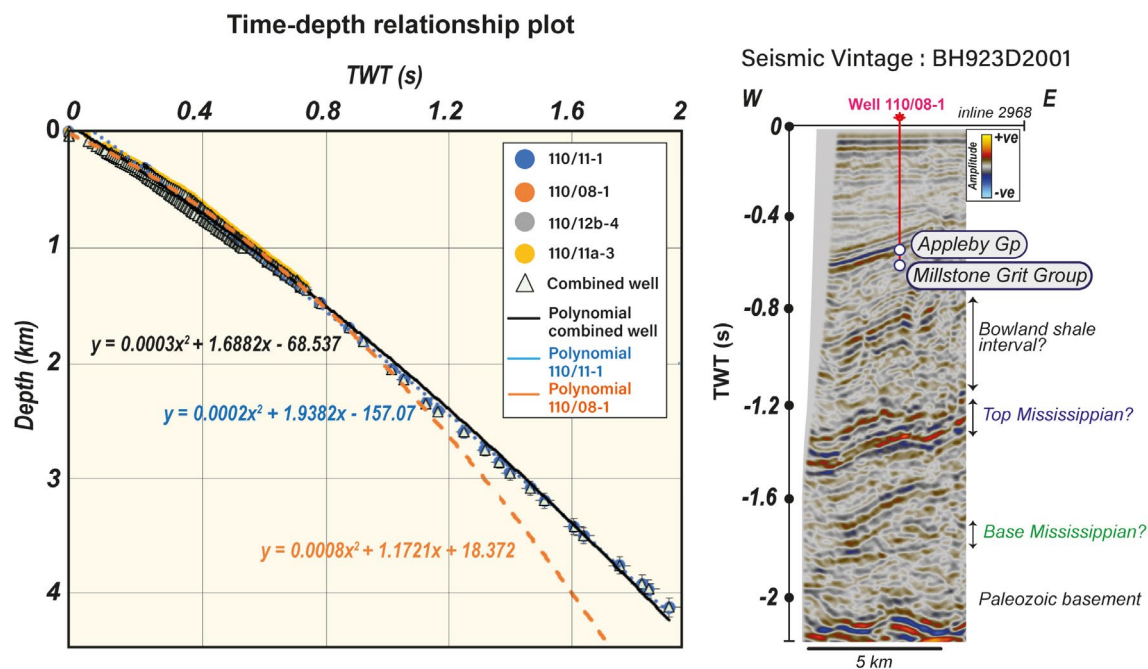| Coverage basin	Seismic vintage	Type	Vertical resolution (m)	Dominant frequency (Hz)	Wells	Depth (m)	Oldest penetrated formation	Interpreter reference
Deemster platform (Hamilton field)	BH923D2001	3D	29	42	110/08-1	1000 (MD)	Miltstone Grit Group (Moscovian)	21CXRM
West deemster basin (WDB)	BG943F0001	3D	62.5	20	110/7a-4	1062 (MD)	Triassic sherwood sandstone fm	BGS
	HY083D0001	3D	56.8		110/08-3	617 (MD)	St Bees Sand (Triassic)	BGS Lithostrat
				24	110/03-2	2394 (MD)	Miltstone Grit Group (Moscovian)	21CXRM
Godred Croven Basin, Godred Croven Platform and Gogarth Basin	ET953F0003	3D	48		110/12b-4	942 (MD)	Sherwood Sandstone	BGS Lithostrat
				26	110/11a-3	1377 (MD)	St Bees Sandstone (Triassic)	BGS
					110/11-1	3508 (MD)	Miltstone Grit Group (Moscovian)	21CXRM
North Wales Offshore	CV933F0001	3D	27	46	n/a	n/a	n/a	n/a
Solway Basin and adjacent areas	Not named	3D	25	45	112/15-1	2616 (TVD)	Brigantian–part of Carboniferous Limestone Supergroup	BGS
	—	—	n/a		M112/19-1	700 (TVD)	Sherwood Sandstone	21CXRM
	—	—	n/a		M111/25A-1	2685 (TVD)	Carboniferous Limestone Supergroup	21CXRM
	—	—	n/a		M111/25-1A	1600 (TVD)	Carboniferous Limestone Supergroup	21CXRM
	—	—	n/a		Silloth 1A	1311 (TVD)	Carboniferous Limestone Supergroup	UK Onshore Geophysical Library

FIGURE 4 | (Left) Time-depth relationship for four wells based on checkshot data from the Southern Irish Sea Basin (EISB). Well 110/11-1 extends to the greatest depth (~4 km), while others reach approximately 1.5 km. A polynomial trend derived from the combined dataset is used to establish an average velocity model, reducing uncertainty by integrating data beyond the deepest well intervals. (Right) Well-seismic correlation for well 110/08-1, a shallow well located in the Hamilton Field (Deemster Platform). Reflection characteristics are examined to validate formation and marker interpretations, particularly for key stratigraphic boundaries such as the top and base of the Mississippian in regions lacking direct well penetration.

TABLE 2 | Time-depth relationship derived from a TWT versus depth polynomial plot. The table includes polynomial equations (*y*) for depth calculations, velocity assumptions at 1800 ms (at 3.5 km depth), depth variations resulting from the ~100 ms error bar and slope angles (*θ*) for different wells. Data is presented for combined well datasets and individual wells 110/11-1 and 110/08-1.

Well	Plot	Velocity assumption at 1800 ms	Depth variation calculation for ~100 ms TWT error bar	Slope angle (*θ*)
Combined well (4 wells)	$y = 0.0003x^2 + 1.6516x - 57.912$	3886 m	531.64 m	27.95°
110/11-1	$y = 0.0002x^2 + 1.9382x - 157.07$	3979 m	546.32 m	28.6°
110/08-1	$y = 0.0008x^2 + 1.1721x + 18.372$	4720 m	810.42 m	39.1°

3.2.1.1 | Implications of Depth Conversion on Dip Estimation. To evaluate the effect of depth-conversion uncertainty on dip estimation, the slope angle (*θ*) was measured along representative platform margins identified on depth-converted seismic sections. These slopes correspond to the upper surface of the Mississippian carbonate platform strata (e.g., A1–A3 in Figure 7) where reflector terminations define the platform-to-basin transition. The slope angle (*θ*) was calculated by measuring the vertical depth difference between the top and base of the platform margin over a fixed horizontal distance of 1 km, following standard geometric estimation from depth-converted grids. This approach provides a first-order estimate of platform-margin inclination rather than an absolute local slope angle, as the available 3D data coverage does not permit continuous cross-sectional profiling along all margins. Extrapolation at 1.8 s TWT yielded depth estimates of 3886 m for combined wells, 3979 m for 110/11-1 and 4720 m for 110/08-1. Using a ±100 ms deviation in TWT, depth differences were calculated (Table 2). The shallowest well (110/08-1) required extrapolation

well beyond the range constrained by available checkshot data and was therefore excluded from subsequent analysis to prevent introducing uncertainty from unreliable velocity trends.

To validate the depth-converted surfaces and further minimise uncertainty, the results of this study were compared with previously published velocity models and depth–time relationships from Pharaoh, Kirk, et al. (2016) and Pharaoh et al. (2018). A previous regression analysis, using field-based average velocities across parts of the EISB, yielded the equation: $y = 0.0003x^2 + 159653x - 103$ (Pharaoh, Kirk, et al. 2016). The combined well model from this study closely aligns with Pharaoh, Kirk, et al. (2016) (Table 2), confirming its reliability. Consequently, the single-well models were disregarded, and the combined well model was selected for depth conversion. The depth conversion and structural mapping were performed using Petrel 2021. The TWT grids were input into the polynomial equation under the depth conversion settings, enabling transformation of seismic data into depth-structure maps (Elam et al. 2020; Kremor et al. 2019).

3.2.2 | Seismic Interpretation of the Top Mississippian Carbonate

Interpreting Mississippian carbonate strata in the EISB from 3D seismic data posed significant challenges due to the relatively poor quality of the data and the absence of well control. Similar difficulties in interpreting Visean strata have been documented in Northern Belgium (Southern North Sea region), as noted by Kombrink et al. (2010) and Reijmer et al. (2017).

Carbonate platforms are hard to identify in frontier settings, as features such as volcanic pedestals or structural highs may mimic carbonate geometries (Burgess et al. 2013; Jiménez Berrocoso et al. 2021). To address this, Burgess et al. (2013) outlined a structured framework for interpreting isolated carbonate platforms using seismic data, focusing on platform-scale morphology, stratigraphic position, internal seismic character and geophysical signatures such as acoustic impedance contrasts. Central to their method is a semi-quantitative scoring system designed to evaluate the presence and clarity of key diagnostic criteria. Each feature is scored based on its interpretive confidence: 1 for a clear positive response (e.g., well-defined mounded geometry, platform margin clinoforms or high-amplitude flat-top reflections), 0.5 for a weak or equivocal response indicating moderate uncertainty, 0 when the criterion cannot be assessed due to limited data or poor seismic resolution and −1 for a clear negative response (Table 4). This score-based approach provides a repeatable and transparent method for assessing confidence in carbonate platform identification, such as those developed on structural highs in low-siliciclastic settings.

To complement this approach, we used the broader observational criteria that describe the seismic characteristics of a wide range of shallow-water carbonate systems, including ramp, rimmed and non-rimmed platforms (Badali 2024). Their compilation provided useful context for recognizing platform types beyond just isolated carbonate platforms. In addition, the study also integrated geological analogues and existing well data to mitigate ambiguities, as recommended by Paumard et al. (2017). To enhance accuracy and minimize uncertainty, seismic interpretation and facies analysis methods were adopted based on techniques detailed by several studies (Hendry et al. 2021; Makhankova et al. 2021; Masaferro et al. 2005) including the use of seismic attributes, such as RMS amplitude (Hendry et al. 2021). This improved the visualization of facies distributions and depositional geometries, aiding the identification of key features within carbonate platforms at the reservoir scale.

The interpretation workflow began with a regional structural framework to define basin geometry, followed by detailed facies and reflector analysis using a merged 3D seismic volume. Interpretation was carried out in Petrel software, applying seismic stratigraphic principles to define two key horizons, the Top Mississippian and Base Mississippian, shown in Figure 4. These surfaces were initially guided by published interpretations (Pharaoh, Kirk, et al. 2016) but were extensively reviewed and re-picked using the higher-resolution dataset available in this study. The Top Mississippian reflector was identified as a laterally continuous peak reflection (increase in acoustic impedance) over structural highs such as the Deemster Platform, where seismic resolution is estimated at ~27 m (Figure 4). The Base Mississippian reflection was of lower amplitude but traceable in areas of better signal quality (Figure 4). Other overlying stratigraphic horizons such as the Appleby Group, Sherwood Sandstone Group, Mercia Mudstone Group and the Base Quaternary were adopted based on reference interpretations (Figure 2; Pharaoh, Kirk, et al. 2016).

Manual horizon picking was conducted at 10–20 trace intervals using loop-tying and crossline validation to maintain consistency across the volume, particularly in areas with variable data quality due to differences in seismic vintage. While this introduces a level of uncertainty, cross-referencing with published maps and reflectivity patterns supports the interpreted picks within the 3D dataset. The presence of Triassic evaporites (mainly halite) in parts of the basin, especially in the central Gogarth Basin, may locally distort the seismic image beneath the salt. However, these evaporites are not widespread across the study area, and their impact is considered spatially limited.

3.2.3 | Fault Analysis

Fault analysis is a crucial component in assessing the evolution of carbonate platforms, particularly in tectonically active, fault-controlled or syn-rift settings (Gawthorpe 1986; Loza Espejel et al. 2019). The interaction between fault kinematics and carbonate platform evolution highlights the importance of structural styles during carbonate platform growth in extensional basins. Temporal and spatial characteristics of fault segments were analysed using time structure and thickness maps, which captured changes in subsidence and accommodation related to faulting and sediment deposition (Duffy et al. 2015). A fault map was generated from 3D seismic data (Figure 7) and further analysed and modelled using a structural workflow in Petrel software. Displacement analysis was performed by constructing displacement-distance profiles, with displacement values measured at 10–20 increments along crossline and inline seismic sections. These measurements spanned a North–South transect approximately 60 km in length. The resulting profiles illustrated variations in displacement across fault surfaces, providing insights into the geometric and kinematic evolution of faults and adjacent folds (Cartwright et al. 2000; Cartwright et al. 1996). To further assess syn-depositional fault activity, the expansion index (EI) was calculated to quantify across-fault stratal thickening. This was achieved by dividing the hanging wall thickness (Ht) of a stratal unit by its corresponding footwall thickness (Ft) and plotting the results against geological time as a proxy for depth (Jackson et al. 2017). An EI value of 1 indicates no across-fault thickening, suggesting an absence of syn-depositional fault activity. An EI > 1 indicates that hanging wall strata are thicker than footwall strata, reflecting active faulting and associated accommodation space creation during deposition. Conversely, an EI < 1 indicates that hanging wall strata are thinner than footwall strata, suggesting thickening towards the footwall, which may result from differential compaction, erosion, carbonate platform growth or footwall uplift (Jackson and Rotevatn 2013).

4 | Results

4.1 | Basin Geometry and Interpretation

The overall interpretation of basin geometry in this study builds on seismic horizon picks from Pharaoh et al. (2018) for all post-Mississippian stratigraphic surfaces. For the Mississippian interval, the base Mississippian and top Mississippian horizons were re-mapped using the available seismic dataset to refine fault geometries and stratigraphic relationships.

4.1.1 | Base Mississippian

In the southern domain of the East Irish Sea Basin (EISB), the basin geometry was analysed along the A–B section (Figure 5), which extends approximately 40 km from west to east. This section is constrained by two wells: 110/11-1, located within the Godred Croven Platform and 110/08-1, situated on the Deemster Platform (Figure 5). The seismic data used for this analysis come from different vintages, resulting in variations in data quality, with the western segment exhibiting lower reflectivity compared to the eastern segment (Figure 5).

The base of the Mississippian has previously been interpreted to lie directly on the Caledonian basement, between 2.5 and 3.0s TWT (Pharaoh et al. 2018). Identifying the Base Mississippian is particularly challenging, however, due to the reduction in seismic frequency and overall poor data quality at greater depths. The interpretation is guided by previous studies (Pharaoh et al. 2018;

Gamboa et al. 2019) and picked at the top of a discontinuous interval of high-amplitude reflectors, which locally transition into chaotic or poorly imaged reflectors (Figures 5 and 6). This inconsistency in reflection character across the study area introduces uncertainty in the pick. On the Deemster Platform, the base Mississippian is identified at ~2s TWT, while in the Godred Croven Basin, it extends to ~2.7s TWT. In the northern domain, the C–D time section reveals that the Base Mississippian also lies significantly deeper than in the south, at up to 2.7s TWT (Figure 6). Within the West Deemster Basin, the base Mississippian is characterised by high-amplitude reflections and moderate continuity.

A depth-converted surface map (Figure 7) highlights the lateral extent and overall morphology of the Base Mississippian. This horizon is regionally continuous across the study area, except where locally truncated by younger unconformities. Three main structural domains are identified: to the south (Godred Croven area and the offshore extension of the North Wales Platform), to the east (Deemster Platform) and to the north (Figure 7). All areas are bounded by relatively low-angle slopes with angles up to 15°. The shallowest occurrences of the base Mississippian are found at approximately −3 km, predominantly within the Deemster Platform, increasing northward to −5.5 km in the West Deemster Basin and Godred Croven Basin (Figure 7).

4.1.2 | Top Mississippian

Mapping the top of the Mississippian surface is also challenging due to variations in seismic data quality across the study area,
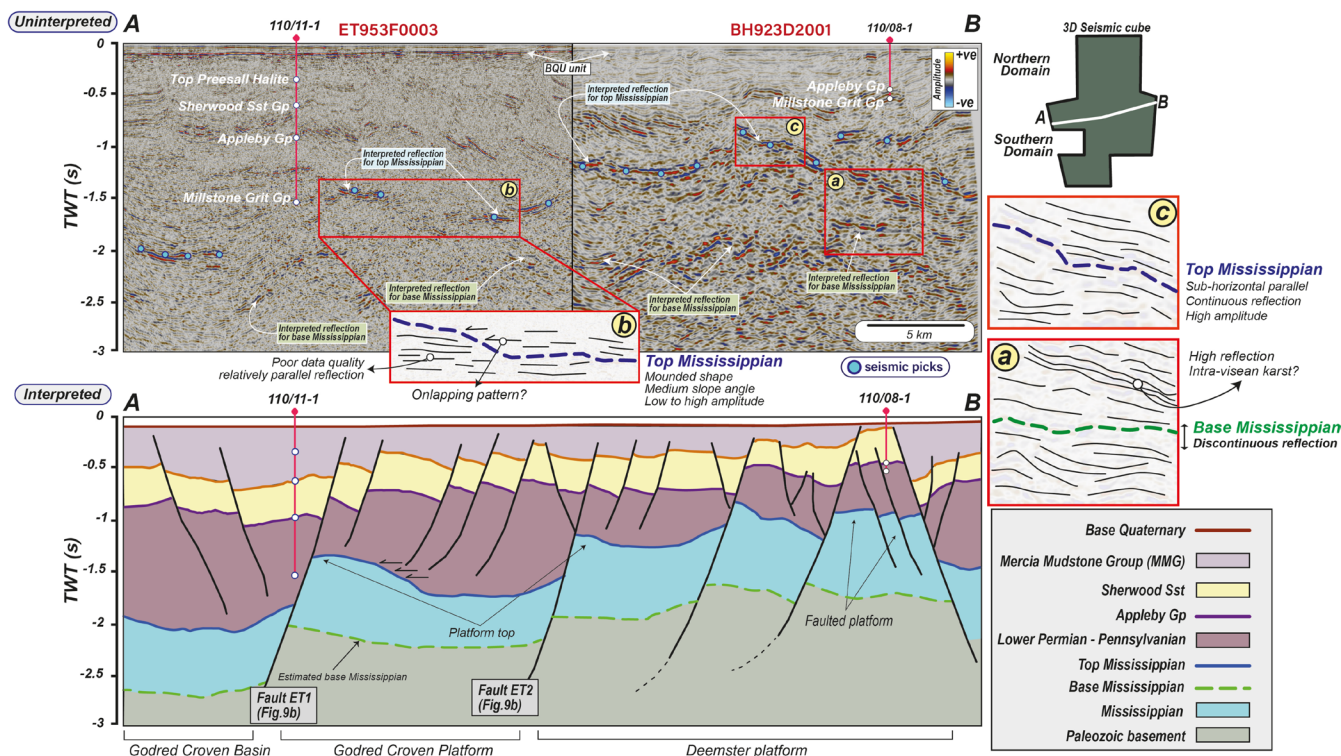

FIGURE 5 | Uninterpreted and interpreted seismic sections along the A–B line, oriented west–east within the southern domain, displayed in two-way travel time (TWT, seconds). The sections show the regional horst–graben architecture, with Mississippian carbonate facies (highlighted in blue) occurring across both platform and basinal settings. A shallow fault cuts the post-Permo-Triassic sequence, primarily affecting the Permian and younger stratigraphy.
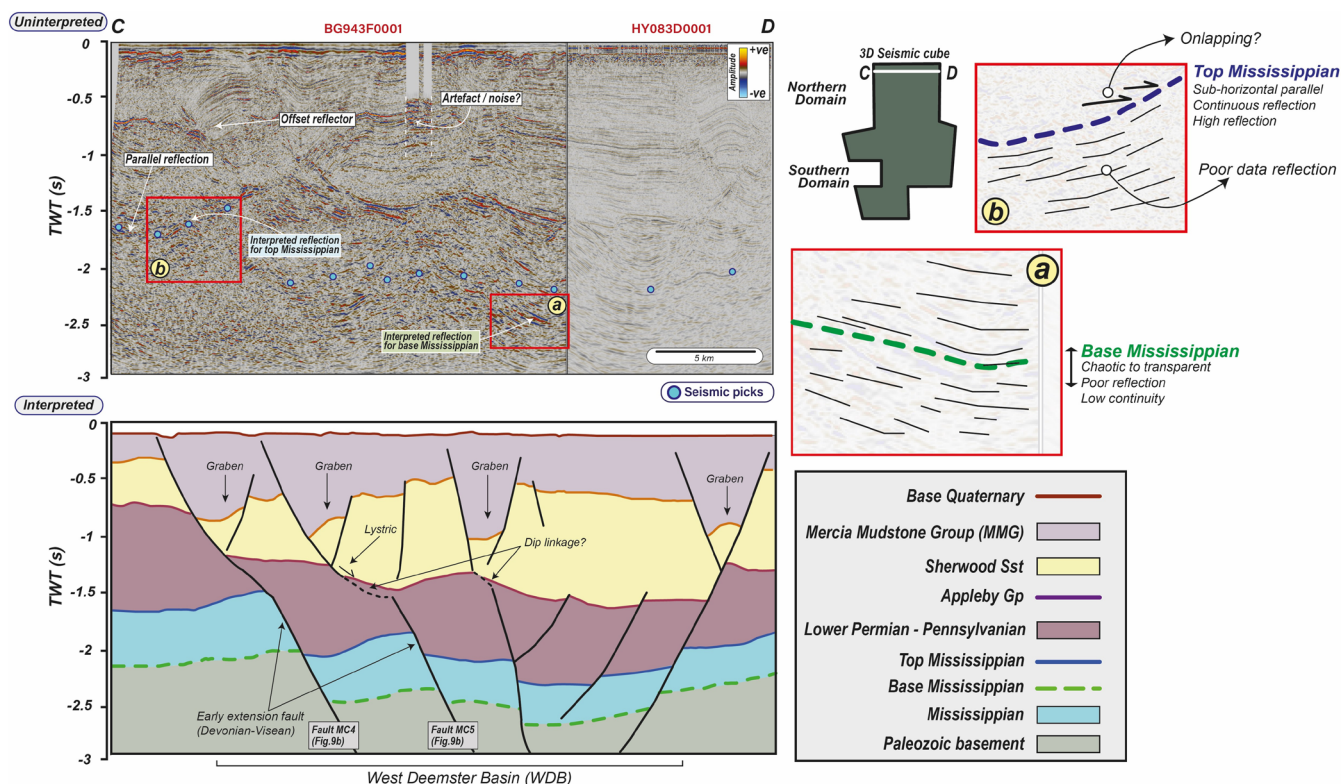
FIGURE 6 | Uninterpreted and interpreted seismic section along the C–D line (west–east) in the northern domain, displayed in two-way travel time (TWT, ms). The Mississippian interval, marked by the blue line, occurs at greater depths here than in the southern domain and shows slight thinning towards the north. The interpretation also reveals a complex network of blind faults, comprising Palaeozoic (Mississippian) faults and post-Palaeozoic (Permian–Triassic) fault systems.

largely influenced by differences in acquisition vintage and processing. Despite these limitations, regional interpretation of multiple seismic sections indicates that this reflector is typically characterized by high-amplitude, continuous and parallel reflections, with localized mounded geometries (Figure 5).

In the southern domain, wells 110/08-1 and 110/11-1, located on the Deemster Platform and the deeper Godred Croven Platform respectively (Figure 5), provide depth constraints that help bracket the position of the Top Mississippian reflector. Although neither well penetrates the Mississippian, they offer an upper limit on its depth, guiding the seismic interpretation in areas of poor reflectivity. On the Deemster Platform, the Top Mississippian is recognised as a high-amplitude, continuous reflection at approximately 1.0s TWT, lying about 0.4s TWT below the base of the Millstone Grit Group. To the west, this surface deepens to around 1.7s TWT (Figure 5). The Top Mississippian also exhibits mounded reflection geometries with a steep slope (~30°), where onlapping reflections from the overlying Pennsylvanian strata can be observed (Figure 5). In the northern domain, particularly along the C–D section in the West Deemster Basin (WDB), the Top Mississippian is mapped at greater depths (from 1.6 to 2.2s TWT) compared to the southern sector (A–B) (Figure 6). Seismic reflections here are generally of poor quality (Figures 5 and 6).

4.1.3 | Mississippian Thickness and Areas

Six discrete areas of localized thickening within the mapped Mississippian interval have been identified across the study

area, labeled A1 through A6 (Figure 8), based on isochore mapping between the interpreted base and top Mississippian carbonate surfaces. Thicknesses were calculated from depth-converted grids using the best fit velocity (Figure 4) in Petrel and are summarized in Table 3. Thickness varies significantly across the EISB, ranging from approximately 1.1–2.0 km, with the thickest areas in the southern and eastern domains (1.8–2.0 km thick; A1–3). In contrast, the northern and western zones (A4–A6) are thinner, generally between 1.1 and 1.35 km thick. Notably, A6, the most northerly zone, is situated atop a structurally elevated horst and exhibits greater thickness and lateral continuity than the adjacent A4 (Figure 8).

Plan-view comparisons between the base and top Mississippian surfaces indicate that several areas have undergone substantial lateral reduction in size over time. For example, A1–A3 originally covered areas between 86 and 213 km² at their base but contract by more than 40% at the top surface (Table 3). A4 and A5 show more modest decreases in area (~12%–18%), while A6 experiences the largest proportional reduction (~47%). Furthermore, thickness diminishes progressively northward across the study area from ~2 to <1 km thickness (Figure 3).

4.2 | Regional Fault Interpretation

Fault visibility in seismic time cross-sections is contingent upon factors such as offset magnitude and reflection continuity. In this study, the quality of seismic data posed challenges for fault
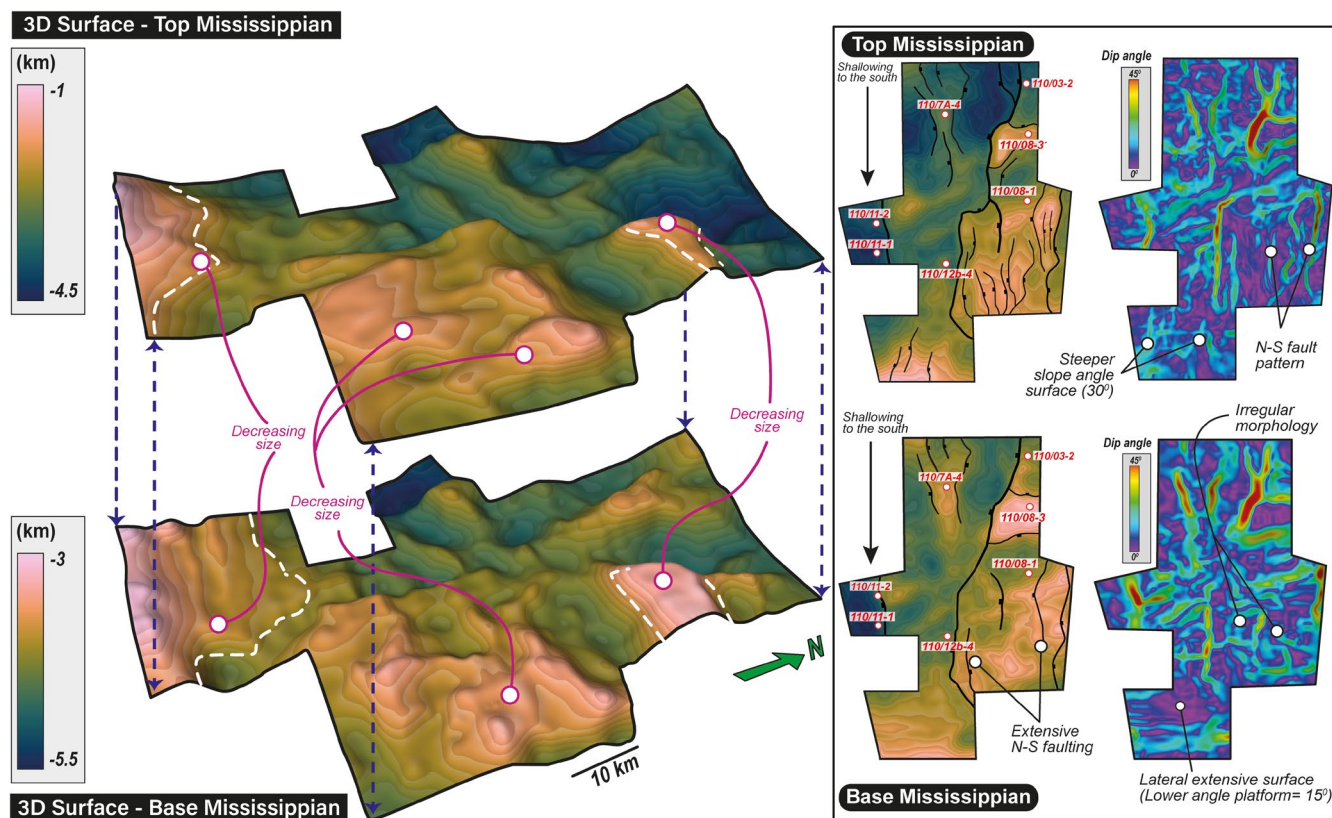
FIGURE 7 | 3D surface interpretation of the top Mississippian carbonate (upper layer) and base Mississippian carbonate (lower layer), shown alongside 2D cross-sections and dip maps in the right panel. The top surface lies at depths of −1 to −4.5 km, with its geometry and distribution closely following fault trends. The base surface reflects irregular platform initiation, characterized by patchy deposition over a broader area and occurs at depths of −3 to −5.5 km.

identification. Nevertheless, analyses of sections A–B and C–D (Figures 5 and 6) provided valuable insights into fault characteristics across the study area. Predominantly, faults affect both the top and base of Mississippian strata and exhibit a north–south (N–S) orientation, with lengths varying between 5 and 40 km. Based on their stratigraphic positions and characteristics, faults were categorized into two groups:

1. Post Permo-Triassic (shallow-seated) faults: These faults are confined to the upper stratigraphic levels, extending into, but not beneath, the Appleby Group (Permian). In the southern domain (section A–B), displacements range from 50 to 100 ms two-way travel time (TWT) (Figure 5). In contrast, faults in the northern domain, particularly the West Deemster Basin (WDB) (section C–D), exhibit greater displacements of 250–300 ms TWT (Figure 5). Notably, in the northern domain, these post-Permo-Triassic faults influence the thickening of the Sherwood Sandstone Group within the basin, forming four mini-grabens (Gamboa et al. 2019). The faults in this region display planar geometries near the surface, transitioning to listric forms at depth as they approach the Permian layers (Jackson et al. 1987).

2. Pre-Permo-Triassic (deep-seated) Faults: These faults dissect the basement, base Mississippian and top Mississippian. In the southern domain (section A–B), displacements range from 150 to 700 ms TWT, with smaller displacements observed within the East Deemster Platform and larger

displacements towards the structurally deeper northern part of the East Irish Sea Basin (Figure 5). In the northern domain, displacements vary between 200 and 700 ms TWT (Figure 6). A notable feature in this area is the linkage between upper (post-Permo-Triassic) and lower (pre-Permo-Triassic) fault systems. Listric faults are evident, and there is strong evidence of a connected fault network linking these two systems (Figure 6). In this domain, areas where faults intersect or connect commonly coincide with localized stratigraphic thinning. This thinning is evident in regions of fault connectivity, expressed as zones of reduced thickness represented by darker colors (Figure 8).

4.2.1 | Fault Growth and Structures in the Mississippian

Understanding the development of Mississippian strata requires that correlations are established between the present-day regional structure, pre-existing formations, stratigraphy and interpreted seismic surfaces. This analysis involved assessing fault throw, fault lengths and the relationship between hanging wall and correlative stratal thicknesses at specific depths, using the expansion index (Duffy et al. 2015; Jackson et al. 2017). A total of 26 faults were identified and interpreted at the Top Mississippian stratal level to examine throw vs. length relationships (Figure 9a). Additionally, measurements of throw-depth variations and expansion index calculations were conducted using seismic horizon picks at the
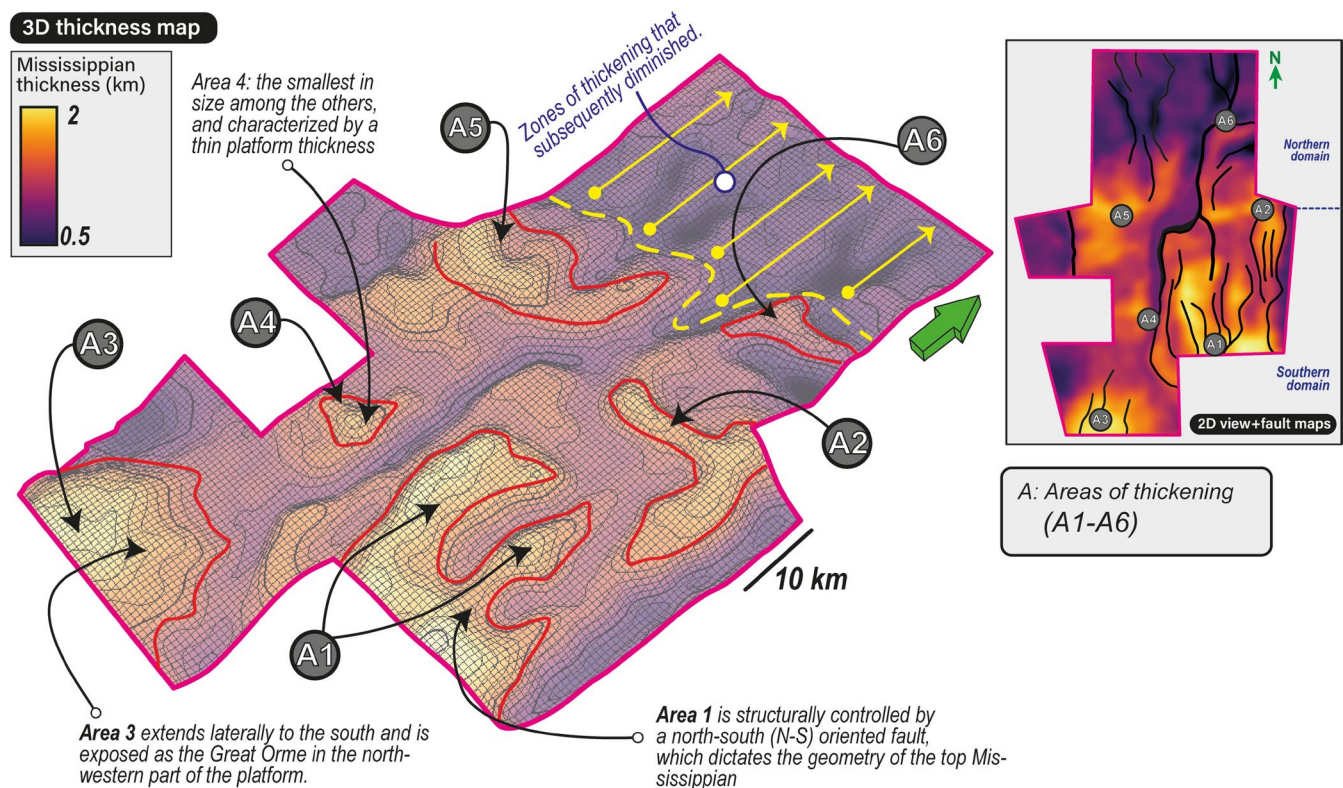
FIGURE 8 | Isochore (thickness) map of the Mississippian interval, illustrating six localised zones of thickening (labelled A1–A6) across the study area. Thickness ranges from approximately 0.5–2.0 km. These zones were identified based on variations between the interpreted base Mississippian and top Mississippian surfaces and are considered candidates for further analysis regarding potential platform development.

TABLE 3 | Geometric and thickness characteristics of the six thickening zones (A1–A6) identified within the Mississippian interval. The table includes the calculated areas at the base and top surfaces (in km²), the percentage reduction in areal extent from base to top (indicating potential platform retreat or truncation) and the maximum thickness (in meters) within each zone.

Parameters	A1	A2	A3	A4	A5	A6
Base Mississippian areas (in km sq)	178.2	86.19	213.91	17.66	45.01	55.74
Top Mississippian areas (in km sq)	92.18	43.68	121.89	15.51	36.68	29.34
Percentage of area reduction	48.27%	49.32%	43.02%	12.17%	18.51%	47.36%
Maximum area thickness (in m)	2000	1850	2000	1100	1350	1200

Top and Base Mississippian levels, complemented by Appleby Group and Sherwood Sandstone Group picks from Pharaoh et al. (2018) (Figure 9b).

4.2.2 | Throw Versus Length Relationship

The dataset shows a positive linear correlation between maximum fault throw and fault length, with a moderate coefficient of determination ($R^2 = 0.52$). This suggests that approximately 52% of the variability in throw can be statistically explained by fault length. However, this does not imply a direct causal relationship, and the remaining scatter likely reflects additional geological factors, including variations in fault growth history, linkage processes and local structural complexities. Several faults in the dataset display relatively high throws for their lengths, which may be due to incomplete imaging of their

full geometries (e.g., MC5, MC4, MC3, HY5) or the presence of features such as breached relay ramps or segmented fault growth. For instance, fault ET6 is a breached ramp, facilitating fault linkage without a clear termination (Figure 9a). These factors can lead to an underestimation of fault lengths and inflated throw-to-length ratios, thereby influencing the overall correlation. Additionally, the observed scatter may reflect variations in fault growth processes, including segmentation, interactions with pre-existing structures or differences in tectonic stress regimes across the study area.

4.2.3 | Fault Scale

The fault scale analysis is derived from the throw distance profile in Figure 9a, which represents a 60 km north–south baseline, where 0 km marks the northernmost point, and 60 km represents
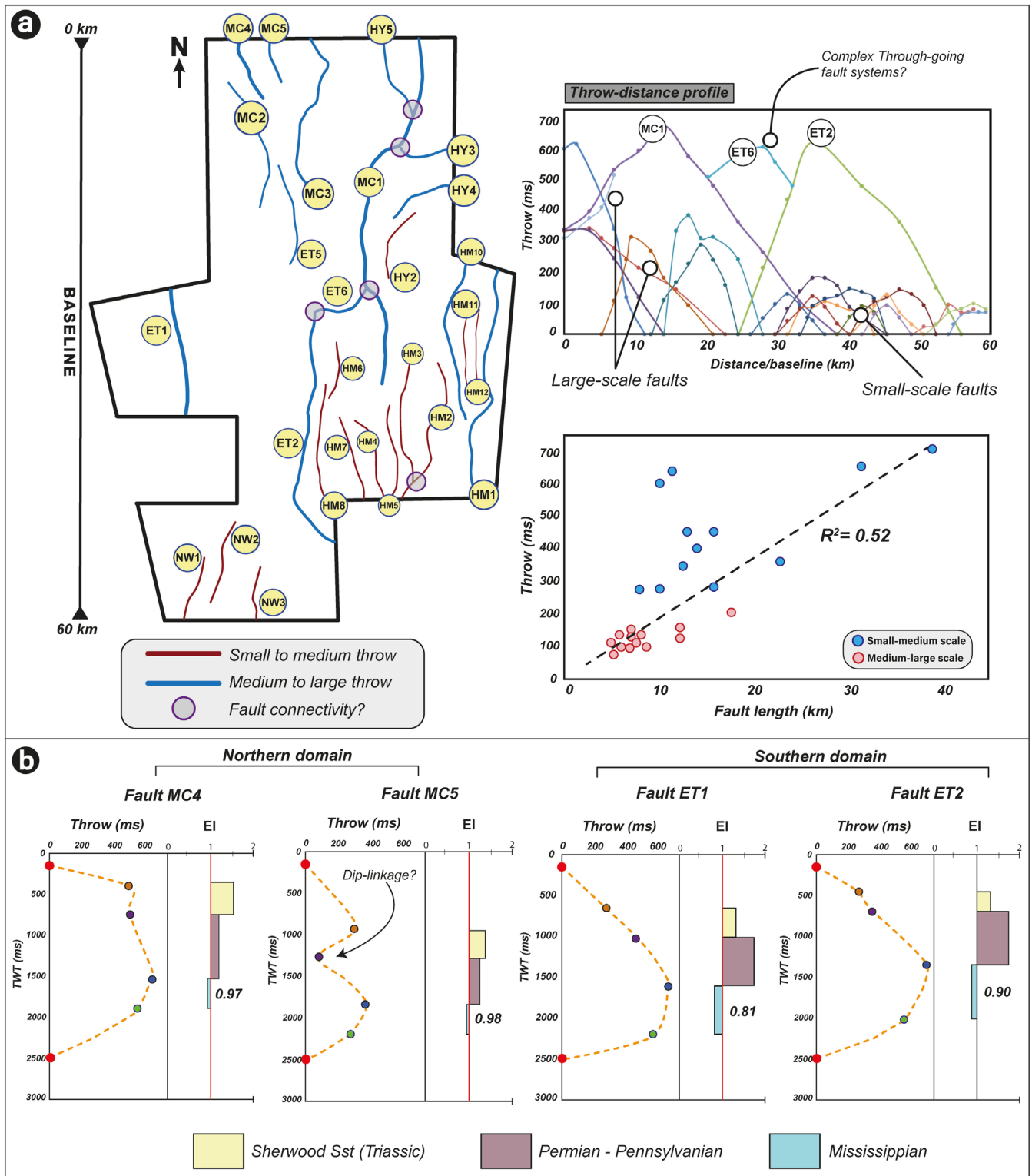
FIGURE 9 | (a) Regional fault map illustrating the distribution and structural styles of faults across the northern and southern domains, with labeled fault names. The inset on the right presents a Displacement-Distance (D-x) plot, highlighting fault evolution behavior, alongside a fault length versus throw graph. (b) Expansion Index (EI) and throw analysis for four faults, tracking their evolution from the Mississippian to the Permian in both the northern and southern domains.

the southernmost extent (Figure 9a). Faults ET1 and HM1 were excluded from the profile due to data limitations, as the polygon cut through these faults prevents observation of their projected fault tips. However, faults with at least one mapped fault tip were included in the analysis.

Structural maps and interpretations categorize faults into two groups: (a) small to medium throw structures, represented in dark red in Figure 9a, and (b) medium to large throw structures, represented in dark blue in Figure 9a. Medium to large (MC1, ET1, ET2, HM1, ET5, MC2, MC4, MC5, HY5, HY3 and HY4)

have fault lengths ranging from 12 to 40 km. Throw values vary between 250 and 690 ms TWT (ca. 0.6 and 1.5 km, given our time depth relationship; Figure 4), and these faults are distributed across both the southern and northern regions.

Faults with small to medium throws are primarily concentrated in the southern domain, particularly in three distinct zones, most of which are spatially associated with structural highs that host thickened Mississippian strata (Figure 9a). Seismic time sections (Figures 5 and 6) indicate that these faults predominantly affect the Top Mississippian reflector, while no clear fault expression is observed at the Base Mississippian surface or within the basement. However, this absence may partly reflect data quality and resolution limitations in the deeper sections. These faults exhibit throw values ranging between ~85 and 200 ms TWT (ca. 0.2 and 0.4 km, given our time depth relationship; Figure 4), with lengths of 5–15 km (Figure 9a). The presence of medium- and small-scale faults within the Deemster Platform influences the position of A1 and A2, as the platform margins appear to align with the N-S fault orientation.

Although most faults trend N-S, fault ET6 exhibits a northeast-oriented direction (Figure 9a). It has a length of approximately 10 km and a displacement of 600 ms TWT (ca. 1.4 km) and appears to function as an intermediate segment linking two major faults, MC1 and ET2 (Figure 9a). Additionally, five potential fault linkages or connectivity zones are identified within the basin (highlighted in purple circles in Figure 9a). However, uncertainties remain regarding the resolution of the seismic data, particularly in accurately mapping fault terminations and confirming linkage connectivity.

4.2.4 | Fault Growth and Stratigraphic Variability

The Expansion Index (EI), as defined by Jackson and Rotevatn (2013), serves as an indicator of stratigraphic thickening across faulted regions. For this analysis, four representative faults were selected in a 3D framework to assess fault growth and stratigraphic variability across different structural domains (Figure 9b). The southern domain corresponds to areas where Mississippian strata are thickest, whereas the northern domain represents areas where the mapped Mississippian is thinner. Key fault parameters were extracted from Petrel and analyzed, including throw magnitude, hanging wall thickness (measured in ms TWT), footwall thickness (measured in ms TWT) and depth of the picked seismic surfaces (in ms TWT).

4.2.4.1 | Northern Domain.
In the northern domain, in the Mississippian interval, the EI is 0.97–0.98, which indicates near-uniform thickness across the fault (Figure 9b). The Permian units show slightly higher EI values, between 1.20 and 1.25, suggesting some differential subsidence during the Permian. This increases within the Sherwood Sandstone to relatively high Expansion Index (EI) values, ranging from 1.35 in fault MC5 to 1.51 in MC4, reflecting strong syn-depositional fault-controlled subsidence and hanging wall sediment accumulation during the Triassic. The throw-depth (T-z) profiles in the northern domain show three key characteristics: (i) no significant thickening across faults in the Mississippian despite a high throw value; (ii) a low throw value in the Triassic (relative

to the Mississippian) and hanging wall thickening; and (iii) dip linkage locally within the Lower Permian Appleby Unit. Fault MC4 exhibits a steady decrease in throw from the Mississippian (~500–600 ms TWT) to the Triassic (~200–400 ms TWT). In contrast, fault MC5 shows a significant throw reduction within the Appleby Unit, followed by an increase in throw magnitude within the lower Triassic (Figure 9b). Seismic time sections illustrate how faults transition from a planar geometry at shallow levels to a listric configuration, before reverting to a planar form in deeper Mississippian intervals (Figure 6).

4.2.4.2 | Southern Domain.
The southern domain is characterised by two linked half-graben geometries, with increasing structural complexity from the Godred Croven Basin to the Gogarth Basin and the Deemster Platform. The Mississippian interval, associated with area A5 (Figures 8 and 9a,b), demonstrates a footwall thickening pattern, with an EI value of 0.81. Similarly, Fault ET2 (Figure 9a) exhibits the same trend, though the Mississippian is shallower, corresponding closely with Area A2 (Figures 8 and 9a); the EI value of 0.90 for the Mississippian interval in A2 further indicates footwall thickening. Both ET1 and ET2 exhibit an increased throw magnitude in the Mississippian, with a subsequent reduction in throw within the Upper Permian–Triassic succession. Fault ET1 (Figure 9b) exhibits significant syn-rift (Expansion Index (EI) values > 1) deformation during the Permian–Triassic, indicating hanging wall thickening. The Throw-depth (T-z) profiles (Figure 9b) reveal maximum throw values of ~680 ms TWT within the Mississippian interval (Figure 9b). Additionally, Fault ET2 appears to function as a fault segment, with MC1 acting as a secondary segment. In summary, the southern domain is characterised by: (i) EI values < 1 in the Mississippian, suggesting greater sediment thickness in the footwall compared to the hanging wall; (ii) greater throw in the Mississippian relative to the Permian–Triassic succession; and (iii) thickening of hanging wall sediments in the Permian–Triassic, as indicated by EI values > 1.

4.3 | Carbonate Platform Characteristics

The identification and characterisation of the areas of enhanced Mississippian stratal thickness (A1–A6) in this study is based on an integrated approach combining regional structural interpretation (Figure 7), fault mapping (Figures 9a,b) and mapping of stratigraphic thickening (Figure 8). This multi-criteria workflow broadly follows the platform identification principles proposed by Burgess et al. (2013), which emphasise the role of geometric expression, internal seismic character and structural context in defining carbonate platforms in the subsurface. In this case, the significant thickness variations observed between platform highs and adjacent depocentres, along with the apparent separation of individual areas of thickening by structural lows, support the treatment of these features as partially isolated entities for interpretive purposes.

Firstly, environmental parameters were considered. During the Mississippian, the study area was situated within shallow water at equatorial to tropical latitudes (Smit et al. 2018), providing favourable climatic and oceanographic conditions for carbonate production and accumulation. This paleogeographic setting was evaluated as key supporting evidence for the likelihood

of carbonate sedimentation (assigned the highest significance score, 1) consistent with models of carbonate platform development in warm, shallow marine environments (Pomar 2001), and the abundance of exposed carbonate platforms of the same age onshore in the UK (Wright 1980; Wright and Vanstone 2001; Somerville 2005; Manifold et al. 2021). There is good evidence onshore and in wells of coeval siliciclastic input into intervening basins between carbonate platforms (Fraser and Gawthorpe 2003).

The geophysical characteristics proposed by Burgess et al. (2013) to be indicative of carbonate strata, received a score of 1 for all platforms based on the presence of a continuous high-amplitude capping reflection. In the 3D datasets from the study area, the top Mississippian reflector exhibits consistently high amplitudes, which are interpreted as diagnostic of carbonate strata due to the strong acoustic impedance contrast between carbonate rocks and the overlying or adjacent sediments (Pharaoh et al. 2018, Pharaoh, Kirk, et al. 2016). All areas of thickened Mississippian strata exhibited a weak positive velocity pull-up (scoring 0.5). This is attributed to the low signal-to-noise ratio (SNR) in the data, making it challenging to distinguish this effect from an underlying antecedent topography beneath the carbonate platforms.

The summary ranking of all areas of thickened Mississippian strata is presented in Table 4 and explained below. In all cases, uncertainties arise in the interpretation of the margins of mapped areas and the base of the interval. The angles of the margins were measured using a depth conversion map generated with the best-fit average velocity method, which introduces potential errors. The identification of the base Mississippian, picked as the lower surface in this study, is interpreted as equivalent to the base carbonate. This interpretation is based on its consistent stratigraphic position beneath the top Mississippian

TABLE 4 | Quantitative scoring of Mississippian carbonate platforms candidates in the East Irish Sea Basin (EISB), based on the criteria established by Burgess et al. (2013). The scoring system evaluates four main criteria subdivided into detailed points, with scores ranging from −1 to +1: +1 indicates a clear positive response, +0.5 represents a weak positive response with some uncertainty, 0 is assigned when the criterion cannot be assessed due to insufficient data, and −1 reflects a definite negative response. Areas A1, A2, A3 and A6 achieved scores exceeding 12, reflecting strong and convincing geological characteristics as carbonate platforms. In contrast, platforms P4 and A5 scored below 10, still displaying carbonate platform geometry but with uncertainty likely dominated by limited data availability or less favorable geological conditions. These findings underscore the utility of quantitative scoring in assessing the potential and geological robustness in the EISB.

		Areas (A)					
Criteria (Burgess et al. 2013)		**1**	**2**	**3**	**4**	**5**	**6**
Regional and stratigraphic constraints	Timing relative to paleolatitude	1	1	1	1	1	1
	Timing relative to regional flooding	1	1	1	1	1	1
	Timing relative to framework builder types	1	1	1	1	1	1
	Location relative to regional tectonic processes	1	1	1	1	1	1
	Location relative to coeval siliciclastic input	1	1	1	1	1	1
Large-scale seismic morphology and basin geometries	Positive antecedent topography (paleohighs)	1	0	1	1	1	1
	Significant localised thickening	1	1	1	0	0	1
	Onlap of overburden or depositional wings	1	1	1	0.5	1	1
	Appropriate isolated areal extent	1	1	1	0.5	1	1
	Absence of equivalent structure in the overburden	1	−1	1	0.5	0.5	1
	High-angle margins	0.5	1	1	0.5	0.5	1
Geophysical characteristics	Continuous high-amplitude capping reflection	1	1	1	1	1	1
	Velocity pull-up	0.5	0.5	0.5	0.5	0.5	0.5
	Absence of gravity and magnetic anomalies	0	0	0	0	0	0
Finer-scale seismic geometries	Margin–related faulting and folding	1	1	1	−1	−1	1
	Buildup margin stacking patterns	1	0	1	−1	−1	1
	Appropriate interior seismic character	1	1	0	0	0	0
	Thick-thin-thick depositional pattern	1	1	1	0	0	0
	Coalescing growth reflection patterns	1	0.5	1	0.5	0.5	0
	Potential karst-related features	1	0.5	0	0	0	0
Total score		17	13.5	16.5	8	9	13.5

in both seismic and well data from the wider surrounding region (e.g., Pharaoh, Kirk, et al. 2016). However, the accuracy of this pick becomes increasingly uncertain with depth due to the limited resolution of seismic data and the lack of direct well control.

4.3.1 | Area A1

Area A1 is located in the southern sector of the Deemster Platform, covering an area of approximately 178 km² (Figure 10a). It extends about 25 km in a fault-aligned south-to-north direction (Figure 10a), placing it > 0.1 probability for platform size as defined by Burgess et al. (2013). Stratigraphic control in this area is limited to a single well, 110/08-1. A seismic section along the A–A′ transect (Figure 10b) illustrates the area's geometry, showing both interior and margin topography, with the top Mississippian reflector occurring at depths of 800–1000 ms TWT.

To analyse the seismic characteristics of A1, an RMS amplitude slice was extracted at 1000 ms TWT, using a 20 ms window centred around each point (±10 ms). The resulting amplitude map displays high-amplitude anomalies (RMS up to 2) in reddish to dark red tones, while lower amplitudes are shown in white (Figure 10a). A subtle NNW–SSE striping pattern is also present, which likely reflects a minor acquisition footprint rather than a geological feature. These high-amplitude zones are interpreted as reflecting the top of the carbonate platform, where a strong acoustic impedance contrast exists between the top Mississippian and the overlying Pennsylvanian strata. Based on well 110/11-1 (Figure 5) and regional studies (e.g., Fraser and Gawthorpe 2003; Pharaoh et al. 2018), the overburden in this part of the basin is assigned to the Bowland Shale Formation, which is predominantly composed of siliciclastic mudstone and sandstone. This lithological boundary produces a prominent positive reflection (peak), consistent with the observed amplitude response across most of the dataset.

The uppermost seismic unit in area A1 is marked by parallel, high-amplitude reflections that produce a flat-topped geometry (Figure 10b). On the platform margins, a transition zone is observed where seismic amplitudes decrease downslope. The northern margin has an average slope of approximately 30°. The southern margin appears more complex, possibly indicating a backstepping feature, with convex-upward reflector geometries with a variable amplitude (Figure 10b). Internally, chaotic and wavy reflections have a thickness of approximately 75–90 ms TWT (equivalent to ~150–180 m) and are centred around 1000 ms depth. This is thickest in the central part of the platform and thins towards the margins (Figure 10b). Other notable features include mounded geometries between 1000 and 1500 ms TWT, with thicknesses of 100–150 ms which are typically located near the platform margin. The internal buildup is observed lower in the succession, with a thickness of 70–100 ms (Figure 10b). The base of the Mississippian has poor seismic resolution, characterised by chaotic to transparent reflections (Figure 10b).

Overall, based on the aspects described above, the large-scale seismic morphology, including a positive antecedent topography, localized thickening, an isolated areal extent, onlap of overburden scored +1. The absence of an equivalent structure in the overburden and the presence of high-angle

margins both support the interpretation of an isolated carbonate platform, thereby increasing the overall confidence score (Table 4). At a finer scale, margin-related faulting, parallel reflectors and convex-upward (mounded) seismic geometries provide good evidence for carbonate strata, with all observations receiving a positive score (+1) (Table 4). These include well-defined seismic reflections typical of platform interior facies, such as mound internal reflections and margin reflections (Figure 10b), buildup stacking patterns and chaotic reflections (Figure 10b). Therefore, A1 overall score reaches up to 17 total score (Table 4).

4.3.2 | Area A2

Area A2 is located approximately 5 km north of A1, separated by an area of lower RMS Amplitude (Figure 10a). A2 has a length of 15 km and covers an area of 86 km², making it smaller than A1. The geometry and structure of A2 are illustrated by the E–W trending seismic section (B–B′), showing that the area is bounded by a series of N–S trending faults that offset the top Mississippian surface (Figure 10c). Faulting within the central portion of A2 affects only the top Mississippian surface and does not extend to the base Mississippian, suggesting that structural control is primarily confined to the upper stratigraphic levels. The margin exhibits steep slopes of 30°. The antecedent topography beneath the area is difficult to identify due to the limited resolution, making it challenging to capture any terminations in the basal part of the succession. As a result, this criterion received a score of 0 in the scorecard (Table 4). However, positive criteria (+1) include the presence of high-angle margins, where faulting controls the margin of the area (Figure 10c), as well as significant localised thickening and thinning from the base to the top of the succession (Table 4).

The top Mississippian is represented by a high-amplitude, parallel reflection at approximately 900–1000 ms TWT (ca. 1.8–2 km). Pennsylvanian strata onlap the margins of Area A2 from west to east, particularly along fault-controlled margins (Figure 10c). These onlapping strata receive a positive score (+1). Below the top Mississippian surface, parallel and continuous seismic reflections become increasingly chaotic, irregular and discontinuous, particularly within a 100 ms TWT interval. RMS amplitude maps reveal localized high-amplitude patches within A2, with amplitude dimming towards the edges of the area, with the internal architecture of A2 exhibiting considerable complexity. At a finer scale, seismic geometries do not show clear evidence of buildup stacking patterns, coalescing growth patterns or potential karst features. As a result, this criterion received a score of 0.5. The overall score for P2 is 13.5 (Table 4).

4.3.3 | Area A3

Area A3 is located in the southernmost part of the study area, immediately offshore of the outcropping North Wales carbonate platform (Figure 11a). The Top Mississippian reflector is characterised by a strong, high-amplitude response in the south, occurring at depths of 550–1500 ms TWT. The amplitude appears to diminish northward; however, part of this variation may reflect differences in data quality and survey calibration across the dataset rather
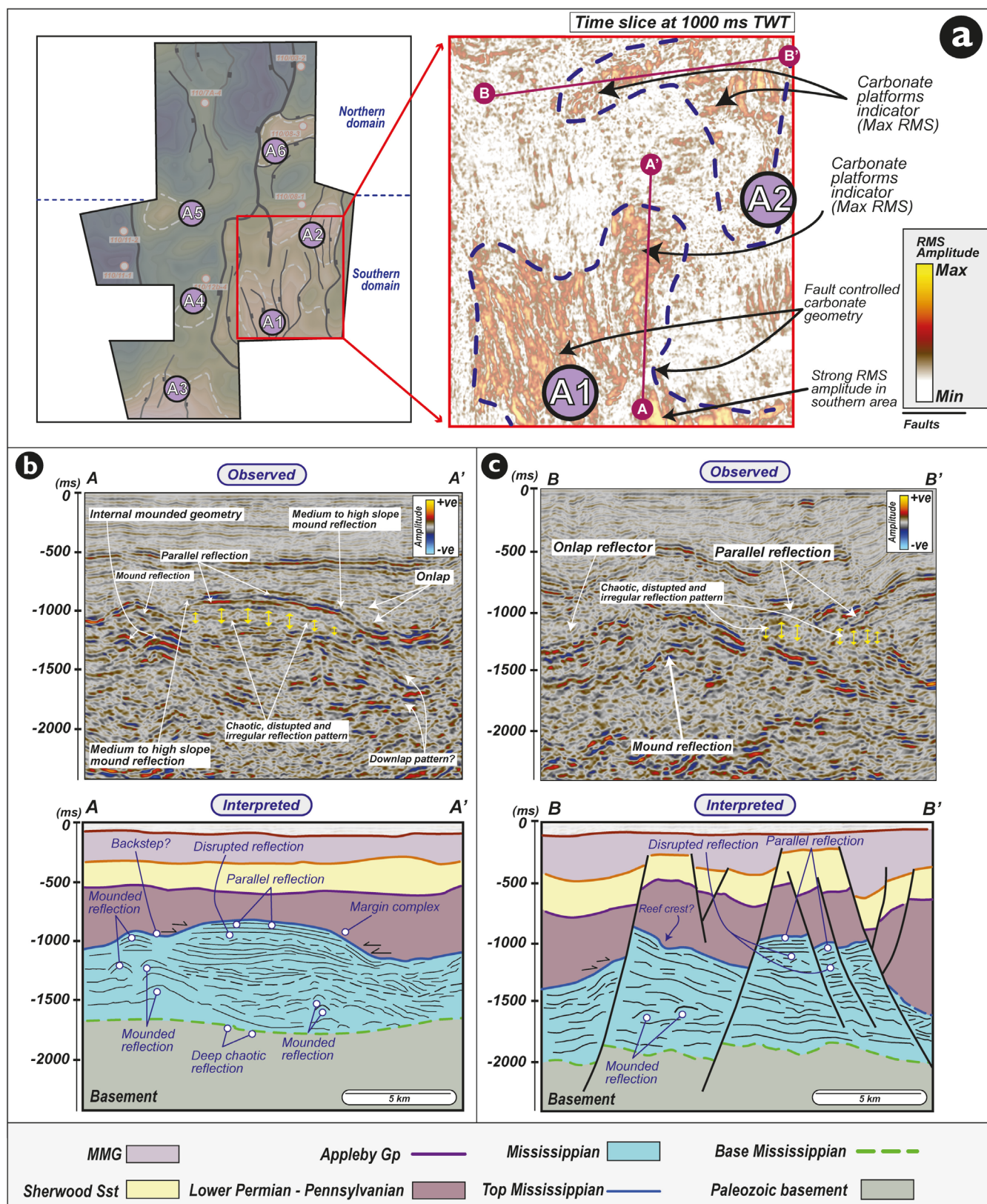
FIGURE 10 | (a) RMS amplitude map from a 1000 ms TWT time slice of the Deemster Platform 3D seismic cube, showing the distribution of carbonate deposits. High amplitudes (red to yellow) indicate concentrated carbonate buildup aligned with north–south (N–S) Mississippian fault trends, while low amplitudes (white) mark inter-platform basins with little to no carbonate deposition. (b) Seismic section A–A′ (south–north) showing the geometry and structural features of area 1 (A1). (c) Seismic section B–B′ (east–west) showing area 2 (A2), highlighting how faulting influenced its development and complex architecture during the Mississippian.
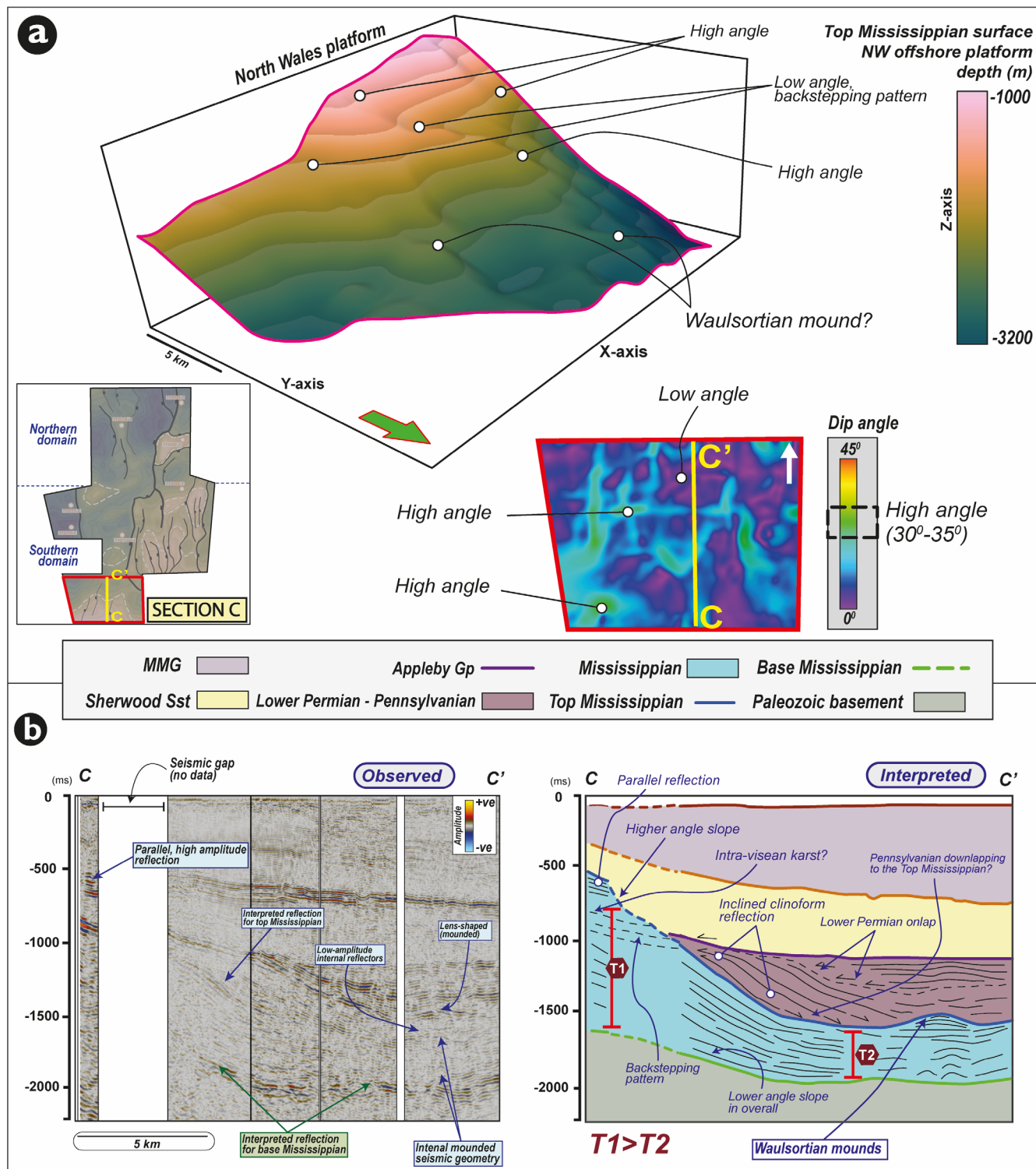
FIGURE 11 | (a) 3D perspective view of the top Mississippian surface in the North Wales offshore area, shown with depth. The platform displays an irregular flat-ramp morphology, marked by slope angle changes, suggesting variable depositional patterns, possibly linked to backstepping during the Visean or late Mississippian. A 2D dip angle map supports this interpretation. (b) Seismic section along line C–C', showing reflection characteristics such as amplitude, continuity and geometry. Key interpreted features include a steepened margin at the top Mississippian, a gentler margin at the base Mississippian and progradational clastics from the Pennsylvanian. The results highlight the interaction between tectonic activity and sedimentation during the Mississippian.

than a true geological change (Figure 11b). To the south, the slope angle ranges between 30° and 35° (Figure 11a). This steep gradient extends approximately 8 km northwards before transitioning into a lower-angle slope (5°–10°). The western part of the area exhibits steeper angles compared to the eastern section, which is more faulted. Evidence of backstepping is apparent in the uppermost

Mississippian strata, where the area at the top of the platform is notably smaller than the underlying area (Figure 11a). Detailed analysis of dip-angle maps reveals an upward transition from a flat or ramp-like section in the lower part of the succession to high angles as the area back-steps to the south, at approximately 200 ms TWT (Figure 11a). Thickness comparison between the southern area (T1) and the northern area (T2) indicates that the southern thickness is nearly twice that of the northern section (Figure 11b). This is corroborated in cross-section, where the base Mississippian exhibits a broad, low-angle dip, while the top Mississippian has a high-angle dip (Figure 11b) that is onlapped by Pennsylvanian strata. Downlap facies are also observed downslope of the top Mississippian in the basin, along with small lens-shaped mounded reflections at the toe of the platform slopes, measuring approximately 100 ms TWT thick (~252 m).

Overall, based on these observations, the scoring for large-scale seismic morphology and basin geometries, following the criteria of Burgess et al. (2013), is entirely positive (+1) (Table 4). However, the seismic interior reflector and chaotic seismic facies criteria received a score of 0, as these features could not be confidently identified in the available dataset due to transparency, resulting from multiple merged seismic cubes with occasional data gaps. Consequently, a score of 0 was assigned for insufficient seismic data (Table 4). The overall score for Area A3 is the highest among all platforms, at 16.5.

4.3.4 | Area A4

Area A4 is situated within the Gogarth Basin, approximately 10 km north of A3 with the top Mississippian surface at a greater depth (approximately 1500 ms TWT; ~3094 m depth based on depth-converted maps) (Figure 12a). Seismic section D–D′, oriented north–south in the southern section, reveals the overall geometry of the platform. A4 is approximately 3–4 km in length and 4 km in width, with a measured area of approximately 17 km² (Figure 12a).

The large-scale seismic morphology displays parallel seismic reflection patterns, while the margins exhibit a mound-shaped morphology with a moderate-angle dip (~20°). These reflections are most prominent along the margin, whereas the overlying strata display onlapping geometries along the margin flanks. Onlap of the overlying Pennsylvanian strata is tentatively interpreted along the northern margin (Figure 12a). As a result, this criterion was assigned a score of 0.5. Additionally, since no isolated areal extent is observed, the margin angle is moderate (~20°) and no equivalent structures appear in the overburden, both criteria were also scored 0.5 (Table 4).

The top Mississippian surface is identified by high-amplitude reflections extending northward, where a smaller mound-like feature is observed at a slightly lower elevation than A4 (Figure 12a). The stacking pattern on the margin and margin-related faulting and folding is assigned a negative score (−1) since these features are not observed in the seismic data and are unlikely to be present. The appropriate interior seismic character and thick-thin-thick depositional pattern were scored 0, as these aspects could not be assessed due to poor data quality (Figure 12a; Table 4).

Several key features characterize A4, including: (a) a medium-angle dip on the margins to the south (~20°) with moderate to high-amplitude mound-like features, (b) onlapping Pennsylvanian sediments onto the margin of the area and (c) a distinct margin or slope break. Overall, A4 received the lowest ranking, with a total score of 8 (Table 4).

4.3.5 | Area A5

Area A5 is located approximately 15 km north of A4 at a slightly higher elevation. It is characterised by the presence of paleohighs observed in the area, which are assigned a score of +1. However, significant localised thickening is difficult to identify, resulting in a score of 0 (Figure 12a). The top Mississippian is picked at approximately 1250 ms TWT (~2475 m depth) within the footwall of a north–south (N–S) trending fault (Figure 12a). Area A5 covers an area of 36.68 km² (Table 3).

The platform margin slope exhibits a high-angle dip (~30°), with medium- to high-amplitude reflections delineating its boundaries. Unlike other areas, there is no significant thickness variation between the platform interior and the adjacent slope or flank strata. As a result, the thick-thin-thick depositional pattern is not distinct and increases uncertainty, leading to a score of 0. The overlying Pennsylvanian sediments that onlap the top Mississippian surface are observed in the southern area and can confidently be identified in the seismic section (Figure 12a).

Margin-related faulting and folding, as well as buildup stacking patterns, are not observed, resulting in a negative score (−1). Interior seismic character is difficult to identify due to seismic data quality limitations, receiving a score of 0. Overall, A5 is ranked slightly higher than A4 due to its larger size and slightly more distinguishable pattern. However, the total score assigned is only 9 (Table 4).

4.3.6 | Area A6

Area A6 is located in the northernmost part of the dataset, along the south–north trending E–E′ seismic section, within the northern domain (Figure 12b). Although situated more northward than other areas, it can be mapped from the base Mississippian to the top Mississippian on a horst block controlled by a network of major N–S trending faults, with additional NE–SW and E–W fault orientations (Figure 12b). The top Mississippian occurs at approximately 800 ms TWT on the horst block and at around 1600 ms TWT in the adjacent deeper basin (Figure 12b).

The base Mississippian of area A6 has a lateral extent of approximately 10 km. However, by the top Mississippian, it has undergone a 47% reduction in size, resulting in dimensions of ~5 km in length and ~7 km in width (Table 3). The area has an estimated maximum thickness of ~1.2 km, with significant localised thickening evident due to fault control. Based on these observations, key criteria such as paleohighs, significant thickening and appropriate isolated areal extent all received a score of +1 (Figure 12b; Table 4).
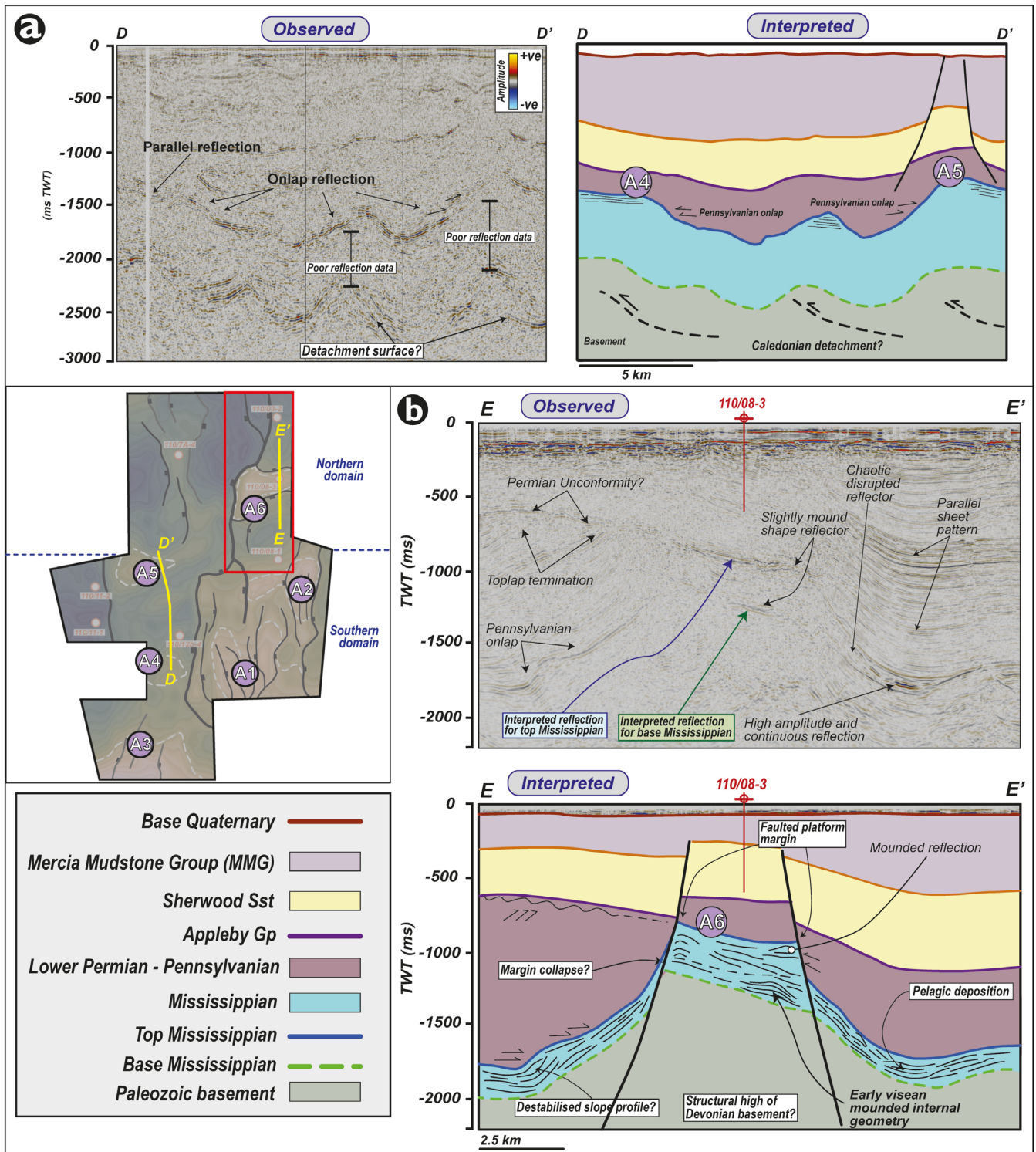
FIGURE 12 | (a) Observed and interpreted seismic section along D–D′, with the left panel displaying the raw seismic data and the right panel showing the interpreted section. Areas 4 and 5 (A4 and A5) are identified within this section. (b) Representative seismic section along E–E′, oriented west to east, illustrating the interpretation of Area 6 (A6). A6 is located in the northern domain at a greater depth compared to platforms in the southern domain. It is positioned within a prominent horst structure at approximately 950–1000 ms TWT.

Seismic reflections within the internal platform structure indicate a slight mounded feature, identified by a reflection with an estimated thickness of 85–100 ms TWT (~214 m) above the base Mississippian surface (Figure 12b). Towards the uppermost part of the Mississippian, seismic reflections transition into consistent, parallel, high-amplitude reflections, although these reflections weaken along the faulted margin. This indicates a decline in acoustic impedance contrast (Figure 12b). These characteristics justify positive scores (+1) for buildup margin stacking patterns and margin-related faulting (Table 4).

Evidence of onlapping remains uncertain due to resolution limitations in the seismic data; however, northern onlapping strata are observed (Figure 12b). The margin of the area exhibits steep slopes exceeding 30° (Figure 12b). The presence of high-angle margins due to faulting and the clear visibility of onlapping overburden justify a score of +1 (Table 4). However, the absence of equivalent structures in the overburden supports the interpretation of an isolated carbonate platform (ICP), as this suggests that deformation is confined to the Mississippian interval. While some internal seismic characteristics are visible, uncertainty remains due to resolution limitations (Figure 12b; Table 4). Overall, Area A6 received a total score of 13.5, ranking it as a strong carbonate platform candidate.

4.4 | Mississippian Carbonate Facies

4.4.1 | Seismic Facies 1 (SF1)-Parallel Seismic Reflection

4.4.1.1 | Observation. Seismic Facies 1 (SF1) is identified predominantly within the southern (A1 and A2) areas (Figure 13). SF1 is characterised by predominantly horizontal and parallel, continuous, moderate to high amplitude reflections. The thickness of this facies ranges from approximately 125–150 ms (TWT) (ca. 0.3–0.375 km, with a depth conversion plot, Figure 4). Laterally, SF1 extends over distances of up to 10–15 km on the top of the platforms. Occasionally, mounded features are observed within these seismic facies, typically manifesting as low-relief, dome-shaped bodies that gently disrupt the otherwise parallel reflector geometry (Figure 13). These mounds exhibit uniformly low to moderate internal reflectivity and lack any distinguishable, stratified internal architecture, suggesting homogenous internal composition. They typically range from approximately 50–100 ms TWT in height (equivalent to ~120–250 m), forming subtle but distinct positive relief features within the otherwise parallel seismic fabric.

4.4.1.2 | Interpretation. SF1 is interpreted as a platform interior facies, characterised by laterally continuous, high-amplitude reflections, suggesting well-lithified and relatively uniform carbonate deposits. The seismic character of consistent amplitude and sub-parallel reflection patterns indicates deposition in a relatively stable platform setting with limited structural disruption (Embry et al. 2021; Pomar 2001). The lateral continuity and stratigraphic positioning of SF1 suggest it is equivalent to bedded, shallow water, subtidal platform top facies on the North Wales Platform which are dominated by crinoidal packstones and grainstones and are stacked into upward-shallowing packages, often capped by emergent surfaces (Juerges et al. 2016; Manifold et al. 2020). The mounded features within SF1 are most likely the internally uniform mounds described by Manifold et al. (2021), which are structureless and dominated by *Siphonodendron corals*.

4.4.2 | Seismic Facies 2 (SF2)—Disrupted Reflection

4.4.2.1 | Observation. Seismic Facies 2 (SF2) is clearly identified a few milliseconds below the top of the Mississippian surface at approximately 100–300 ms (TWT) (ca. 0.25–0.7 km, with a depth conversion plot, Figures 4 and 13). SF2 was only clearly observed within area A1 and is characterised by localised low to medium amplitude (Figure 13). The internal reflector configuration appears chaotic, with an overall sub-parallel but disrupted pattern. The thickness of this facies varies, but the average observed interval is 50–70 ms TWT, corresponding to an approximate average thickness of 120 m.

4.4.2.2 | Interpretation. SF2 is interpreted as a zone of karstification (Figure 13), based on its chaotic to disrupted reflectors, abrupt lateral terminations and localised zones of reduced amplitude continuity. These features differ from the lower reflector coherence seen elsewhere in the dataset and are interpreted as potential indicators of collapse or dissolution structures commonly associated with karst processes (Hu et al. 2023). It is important to note that the resolution of the seismic data varies from approximately 25 m in the better-quality cubes to 62.5 m in others (Table 1). While individual karst conduits or small-scale solution features are likely to be below the limit of seismic resolution, the broader seismic response namely the chaotic character, diminished amplitude and internal vertical collapse features of SF2 are consistent with previously published examples of karst-related seismic facies (Hendry et al. 2021). It is possible, therefore, that it represents a complex interval of multiple phases of downcutting fissures and collapse structures, perhaps associated with a significant period of relative sea-level fall. One possible interpretation is that the interval reflects a period of emergence and exposure that has been well described onshore at the Asbian—Brigantian boundary (Somerville and Strank 1984; Manifold et al. 2021; Gutteridge 2024), or an older event that has not been identified in outcrop.

4.4.3 | Seismic Facies 3 (SF3)–Mounded Seismic Reflection

4.4.3.1 | Observation. Seismic Facies 3 (SF3) exhibits a distinctive mound-shaped geometry, characterized by moderate to high amplitude reflectors with a convex-upward morphology (Figure 13). The mounded structures appear irregularly distributed along the platform margins and display notable lateral variability in internal architecture. The average mound slope thickness is approximately 150 ms (TWT) (ca. 0.375 km), though some buildups exhibit localized thickening (Figure 13). SF3 is consistently observed across areas with varying degrees of seismic resolution affecting the clarity of internal facies architecture. In higher-resolution sections, internal reflections appear semi-continuous to chaotic, with evidence of inclined reflectors within the buildup. The lateral extent of individual mound-shaped features varies, typically ranging between several hundred meters and over a kilometre, depending on the degree of platform margin development and the depositional setting.

4.4.3.2 | Interpretation. SF3 is interpreted primarily as a carbonate platform-margin buildup complex, based on its convex-upward geometry, limited lateral continuity and proximity to the slope break. These features are consistent with reefal or marginal buildups, where carbonate production and sediment accumulation were focused along the platform edge
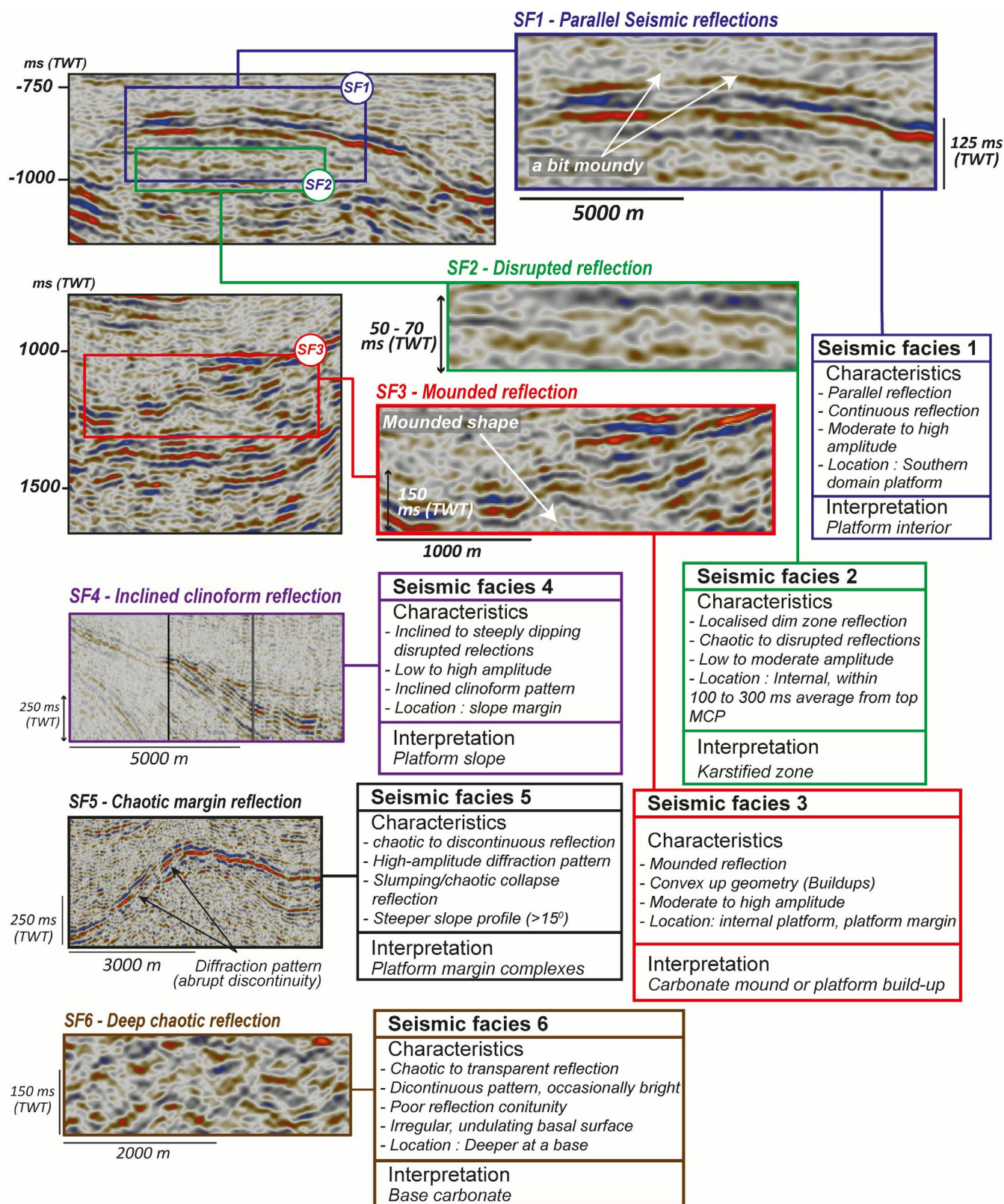
FIGURE 13 | Seismic facies (SF1–SF6) identified from 3D seismic reflection data across the East Irish Sea Basin (EISB), integrating observations from both the southern and northern domains. Each facies exhibits distinct reflection characteristics, including variations in internal geometry, shape, amplitude and reflection continuity. These facies highlight key differences in the internal architecture, depositional geometry and overall morphology of the Mississippian.

(Bashir et al. 2021; Chee et al. 2018). Similar facies configurations have been documented in seismic studies of carbonate platforms, where mound-shaped buildups with moderate to high-amplitude reflectors are associated with both platform-margin complexes and localised buildups within the platform interior (Eberli and Betzler 2019; Zampetti et al. 2004). Such mound-shaped

features are also recognised within the internal parts of carbonate platforms, where localised environmental conditions such as elevated productivity, topographic highs, or ecological niches favoured the formation of isolated carbonate mounds (Burgess et al. 2013). That this facies usually marks the transition from the platform top to slope environment is further evidenced by the change from parallel to inclined reflectors. The inclined reflector within the mounds suggests progradation and vertical accretion, typical of a healthy carbonate margin. Discontinuous massive, domal mounds comprising crinoids, brachiopods and bryozoa have been described from the late Visean of the northern margin of the Derbyshire Platform and the Askrigg Platform, marking the transition from platform top to slope (Mundy 1992; Manifold et al. 2021). They are smaller and thinner than the features described here from seismic (typically ~30 m thick; Mundy 1992), suggesting that the seismic facies reflect the coalescence of numerous smaller mounds.

4.4.4 | Seismic Facies 4 (SF4)–Inclined Clinoform Reflection

4.4.4.1 | Observation.
Seismic Facies 4 (SF4) is prominently observed in the southernmost areas particularly along the slope margin of area A3 (Figure 13). These facies are characterised by semi-parallel, inclined and disrupted reflections, displaying a distinctive clinoform pattern with sigmoidal geometry and downlapping terminations dipping northward (Figure 13). The reflectors range from low to high amplitude. This facies is positioned downdip of the platform margin, extending laterally for up to 10 km. The observed slope angles range from approximately 20°–30°.

4.4.4.2 | Interpretation.
SF4 is interpreted as an inclined clinoform facies representing the onlapping Pennsylvanian deposits that define the slope geometry of the underlying Mississippian platform margin (Figure 13). Although not part of the Mississippian succession itself, this facies provides valuable evidence for the orientation and configuration of the platform slope due to its close stratigraphic association. The sigmoidal clinoform geometry, semi-parallel reflections and downlapping terminations are consistent with slope progradation into the basin (Pomar 2001; van Hulten 2012; Bachtel et al. 2005; Van Tuyl et al. 2018). The observed variations in reflection amplitude likely indicate prograding sedimentary bodies composed of mixed carbonate–clastic material deposited during early Pennsylvanian transgression. Given the limited well penetration and seismic resolution in this southern area, the inclusion of SF4 helps constrain the slope morphology of the Mississippian platform margin. Comparable progradational geometries have been documented in similar transitional settings, such as along the margins of the Derbyshire and North Wales Platforms (Manifold et al. 2021), where post-Mississippian strata onlap earlier carbonate platforms.

4.4.5 | Seismic Facies 5 (SF5)–Chaotic Margin Reflection

4.4.5.1 | Observation.
Seismic Facies 5 (SF5) is observed predominantly along the margin and slope areas of mapped areas (A1, A2, A6). This facies is characterised by chaotic to discontinuous reflections, with high-amplitude seismic signatures and the presence of diffraction patterns along the slope (Figure 13). The internal seismic character exhibits slumping or chaotic reflections, particularly in the steeper sections of the slope. The slope profile exceeds 15°, and the thickness interval of SF5 is approximately 150 ms (TWT) (ca. 0.375 km). Laterally, this facies extends for between 1 and 2 km, indicating a localised but laterally constrained feature. The transition from relatively more continuous reflections upslope to chaotic reflections downslope suggests a marked break in stratigraphic or depositional continuity. Although discontinuous reflections are present elsewhere in the dataset due to general limitations in data resolution, the spatial confinement and consistent morphology of SF5 distinguish it from background noise or artefacts.

4.4.5.2 | Interpretation.
SF5 is interpreted as a platform margin collapse complex, due to the presence of chaotic seismic reflections which suggest instability. The material is interpreted to have been transported from the platform margin, downslope forming a debris apron or mass-transport deposit. It likely resulted from slope failure, gravitational instability or syndepositional tectonic activity. Similar facies configurations have been documented in seismic studies of platform margin collapses, where high-amplitude chaotic reflections, diffraction patterns and disrupted geometries are indicative of mass-wasting processes (Etienne et al. 2021) These collapse features can vary significantly in scale, ranging from less than a kilometre to tens of kilometres across, leading to substantial bankward margin retreat and the redistribution of carbonate debris downslope (Lukasik and Simo 2008). Kirkham (2021) interpreted disrupted, slumped facies and slide planes along faults in the Halkyn area of North Wales, while Davies (2008) interpreted a megaslide affecting Brigantian and Serpukhovian strata on the northern margin of the exposed North Wales platform, supporting the interpretation of a platform margin collapse complex.

4.4.6 | Seismic Facies 6 (SF6)—Deep Chaotic Reflection

4.4.6.1 | Observation.
Seismic Facies 6 (SF6) is observed at the base of the Mississippian carbonate succession (Figure 13). This facies is defined by chaotic to semi-chaotic seismic character, marked by a lack of coherent, laterally continuous reflectors. The reflections exhibit an undulating and irregular geometry, forming a distinct basal reflector beneath the overlying carbonate platform deposits. Localized zones of high amplitude 'bright spots' are intermittently present, but their geometry is irregular and spatially discontinuous. The basal contact between SF6 and the overlying carbonate platform is undulating and in places difficult to trace due to the limited seismic signal quality at greater depths. SF6 becomes especially dominant in areas where the base carbonate pick approaches the deeper part of the basin, around 2.5–3.0 s TWT, where signal attenuation increases.

4.4.6.2 | Interpretation.
SF6 is interpreted as the base of the Mississippian carbonate succession (basal carbonate). Similar facies configurations have been documented in basal carbonate settings, where deep chaotic reflections are commonly associated with deeply weathered or highly heterogeneous

substrata (Fraser and Gawthorpe 1990). The undulating nature of the basal reflector suggests that SF6 may correspond to an irregular paleo-topography, possibly reflecting a pre-existing siliciclastic or volcaniclastic substrate. The discontinuous seismic character further supports the interpretation of a heterogeneous lithology or a highly compacted substrate, which could have influenced the initiation of carbonate platform growth (Fyhn et al. 2013).

5 | Discussion

This study has identified six areas of possible carbonate platform development (A1–A6) based on seismic observations and ranking based on predefined criteria (Burgess et al. 2013; Table 4). All platforms scored positively in the confidence assessment (i.e., they display characteristics consistent with carbonate platform geometry and seismic facies following criteria adapted from Burgess et al. 2013). Areas A1, A2, A3 and A6 scored strongly (≥ 12; Table 4), based on well-imaged seismic expressions of platform tops, margins and internal architecture. In contrast, areas A4 and A5 received lower scores (8–9), reflecting deeper depths beneath the surface, poor seismic resolution, ambiguity in delineating platform boundaries. These confidence scores indicate relative certainty in platform identification, not necessarily a judgement on the completeness or productivity of the platform itself (Burgess et al. 2013).

5.1 | Timing of Faulting and Tectonic Framework

Understanding the complex structural framework of the study area is pivotal in unravelling the growth and geometry of carbonate platforms during back-arc extension during the Mississippian in northern England. This back-arc basin is interpreted to have formed under broadly N-S oriented extension, northwards of the Variscan orogenic belt (Jackson et al. 1997; Fraser and Gawthorpe 2003; C. N. Waters 2009; Smit et al. 2018). However, detailed seismic mapping of the East Irish Sea Basin in this study reveals that predominantly north-south (N-S) trending extensional faults, identified at both the Base Mississippian and Top Mississippian surfaces, apparently controlled carbonate platform growth (Figures 5–7). This is inconsistent with a broadly N-S oriented extension inferred by regional studies (Smit et al. 2018). There are two possible explanations for this: (1) the faults formed during back-arc extension in the Mississippian, but inherited the underlying basement structural trend, perhaps reflecting local variations in regional stress (Needham and Morgan 1997; Worthington and Walsh 2011; Smit et al. 2018), or (2) the faults formed during E-W extension in the Mesozoic but are rooted in the Mississippian. In this case, the faults would have formed after carbonate platform growth and could not have controlled carbonate sedimentation.

The assessment of displacement against distance profiles was undertaken to try and resolve these possible interpretations. Large-scale faults, with their extensive displacement, could have had a transformative impact on basin architecture, leading to substantial changes in its overall shape and structure as is shown in the linkage between fault ET2, fault ET6 and fault MC1 (Figure 9). Small to medium scale faults, could have also had a pronounced

effect, introducing significant changes to basin morphology over a shorter distance (Figure 9). These faults may have exhibited localised and more limited displacement, resulting in less significant changes to the basin's shape than the larger faults (Figure 7). The vertical profiles of expansion and throw analysis provide valuable evidence of offset along faults during the Mississippian (Figure 9a). For example, faults ET1 and ET2 show Expansion Index (EI) values (Jackson et al. 2017) less than 1 in the Mississippian, indicating thicker sedimentary strata in the footwall compared to the hanging wall (Figure 9b). This suggests that during this time, tectonic activity or subsidence patterns favoured sediment accumulation on the footwall. This is consistent with Fraser and Gawthorpe (2003), who showed that Mississippian carbonate platforms across the UK grew on structural highs, where shallower water facilitated carbonate platform growth. In contrast, for most of the Triassic–Permian (Figure 9b) sedimentary package, EI values are >1, indicating thicker sediment accumulation in the hanging wall, typical of syn-rift basin development in a clastic-dominated basin associated with active faulting. This is consistent with E-W extension and hanging wall subsidence during this period (Jackson et al. 2017; Jackson and Rotevatn 2013; Peacock et al. 2018).

Further evidence for syn-depositional faulting in the Late Mississippian (Visean) is shown by the dip linkage originating from Fault MC5 (Figure 9b). The substantial throw on this fault (up to 435 ms; Figure 9), suggests that it grew during the Devonian–Mississippian. In comparison, the throw on this fault in the upper layer of the Triassic is 250 ms (Figure 9b). The displacement of the lower segment (Tournaisian–Visean) exhibits an asymmetric pattern, with a gradual decrease in throw, implying that the fault propagated beneath the surface, remaining blind (Jackson et al. 2017; Jackson and Rotevatn 2013). During the Permian–Triassic, the fault was reactivated and breached the surface, evidenced by a significant decrease in throw profiles, to 100 ms (Figure 9b).

Overall, seismic interpretation of the southern EISB indicates that carbonate platform growth occurred offshore of the principal, land-attached North Wales carbonate platform, but was irregular and strongly fault-controlled, particularly in proximity to major structural lineaments (Figures 7 and 9a). The alignment of carbonate platform margins with N–S-trending faults, and calculation of expansion indices, strongly suggest a tectonic control on platform growth, with footwalls providing structural highs for preferential carbonate accumulation (Figure 7). Similarly, fault control on platform carbonate development has been widely recognised in Mississippian basins globally (Jutras et al. 2016; Koehl et al. 2023) including in the North Atlantic margin (Worthington and Walsh 2011), The Netherlands and Belgium (Gutteridge et al. 2025; Kombrink et al. 2010; Reijmer et al. 2017).

5.2 | Distribution of the Mississippian Carbonate Platforms

The overall structural and stratigraphic framework of the EISB has been documented (Pharaoh et al. 2018, 2021), but while these studies established the tectonostratigraphic evolution of the basin, they did not provide a detailed assessment of the geometry, spatial distribution and size variability of potential carbonate platforms.

In contrast, this study reveals a complex platform–to–basin transition from the North Wales carbonate platform into the East Irish Sea Basin; rather than a simple platform margin slope there is a gradual restriction of carbonate growth to footwall highs. In the south of the study area, the platforms have complex terminations with numerous promontories and embayments (A1–A3; Figure 8), while further north carbonate platforms are smaller, more isolated and exhibit a simpler morphology (Figure 14).

Differential growth between the footwall and hanging wall can be attributed to the interplay of tectonism, water depth and environmental conditions (Masiero et al. 2021). The EISB is > 35 km northwards of the Wales-Brabant Massif, which controlled the influx of clastic sediment onto the North Wales Platform in the Tournaisian and Visean, and this clastic input periodically interrupted carbonate platform growth in the most proximal areas of the platform (del Strother et al. 2021; Manifold et al. 2021). Within the EISB, there would also have been input of siliciclastic sediments from the north and west, such as via the Bowland (Craven) Basin and the Solway Basin (Fraser and Gawthorpe 2003). The most southerly areas (A1 and A3) score most highly for probability of carbonate platform development, followed by A2, which is just to the north of A1. This suggests that these areas had the most optimal conditions for carbonate platform growth, with

higher light penetration due to greater tectonic stability and/or lower clastic input (Reijmer 2021; Weij et al. 2019). Conversely, those areas that score lower for carbonate platform development (A4, A5 and A6) occur further offshore from the North Wales Platform. Here, the top Mississippian surface is picked at deeper depths than A1–3, Mississippian strata are thinner and the areas of the platforms are smaller (Table 3). This suggests that conditions for carbonate platform development were sub-optimal, reflecting their location in a more distal setting and hence deeper water, relative to the North Wales Platform. They might also have been influenced by clastic input from the north and west. Under these conditions, the platforms would have had to aggrade to keep up with sea level. Furthermore, the absence of evidence for karst (SF2) in these areas suggests shorter periods, or an absence of, platform emergence and karstification.

All six areas (A1–A6) show evidence of a significant reduction in area (up to 49%) from the base to the top of the Mississippian succession (Table 3). This progressive backstepping suggests that all platforms reduced in size in response to changing environmental conditions from the Tournaisian to the Visean. This change in platform size occurs across the study area and has also been observed within carbonate platforms onshore, with a termination of carbonate platform
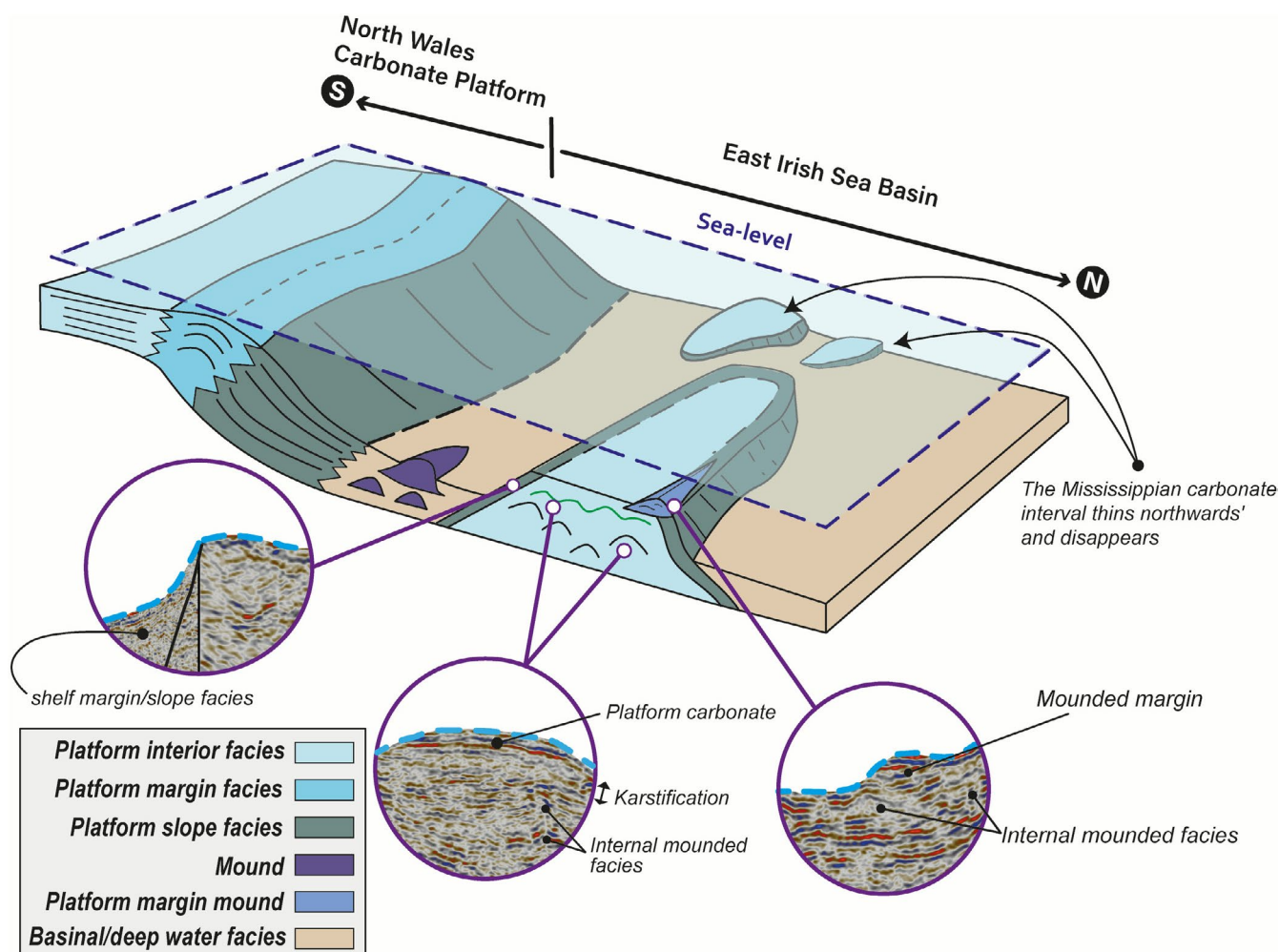

FIGURE 14 | Three-dimensional (3D) schematic conceptual model of the northern ward margin of the North Wales Platform in the southern East Irish Sea Basin.

growth in the late Visean across the Pennine Basin (Fraser and Gawthorpe 2003). For example, on the Derbyshire and North Wales Platforms there is a change in facies and back-stepping of the platform margin in the Brigantian (Juerges et al. 2016; Manifold et al. 2021).

5.3 | Basin Development and Its Control on Carbonate Platform

The distribution of Mississippian carbonate platforms in the East Irish Sea Basin can be characterized by four distinct stages (Figure 15), interpreted by the analysis of mapped surfaces, internal and external seismic facies characteristics and fault analysis.

5.3.1 | Platform Initiation (Tournaisian)

During this early syn-rift stage, back-arc extension initiated the differentiation of footwalls and hanging wall basins (Leeder and Gawthorpe 1987; Coward 1995; Fraser and Gawthorpe 2003), with the initiation of carbonate platform deposition in the Tournaisian north of the Wales-Brabant Massif in shallow marine settings (Somerville et al. 1989; C. N. Waters 2011). Throughout the Mississippian, the equatorial position of northern England, combined with low clastic input, played a crucial role in facilitating extensive carbonate production and platform growth on low- to moderate-angle carbonate ramps to low angle, flat-topped platforms (Somerville et al. 1989; Somerville 2008). Rare exposures and borehole data onshore (e.g., Schofield and Adams 1985) interpret shallow water, open marine sedimentation immediately offshore of tidal flat complexes. Within the study area, slope angles of ~10°–15° are observed in areas A1, A2 and A3 (Figures 10 and 11), implying some distal steepening of the platforms, perhaps due to faulting or differential compaction. The progradational nature of the Mississippian platforms, suggests a prolonged phase of high carbonate productivity and significant offshore sediment transport, particularly in area 3 (A3) (Figure 11). Mounded facies (SF3) developed on the platform top within the most proximal platforms (e.g., A1; Figure 10), although most platforms are dominated by laterally continuous, bedded facies.

5.3.2 | Platform Growth (Tournaisian—Mid Visean)

By the mid-Visean, carbonate platform development was becoming more spatially restricted, as observed by A1, A2, A3 and A6 (Figures 10–12). This is consistent with the transition from ramp to rimmed shelf morphologies seen within many carbonate platforms onshore and worldwide (Barnaby and Read 1990; Burchette and Wright 1992; Della Porta et al. 2004; Gómez-Pérez et al. 1999; Waters et al. 2017). The corresponding decrease in the mapped platform areas in this study could have been driven by both a change in relative sea level and environmental change. Onshore, carbonate platforms thrived throughout much of the Visean, with platform growth interrupted only by periodic emergence (Wright and Vanstone 2001; Manifold et al. 2020, 2021). At the same time, fault analysis in this study shows that active faulting, continued to influence carbonate accumulation, with the expansion index (EI) of 0.8 and 0.9,

suggesting continued carbonate growth on the footwall of N-S trending faults. It is therefore likely that the steepening of the carbonate platforms reflects, at least in part, tectonic activity. On a regional scale, differentiation of the largest platforms, such as the Derbyshire and Askrigg Platforms, continued as hanging wall subsidence was facilitated by extensional tectonics (Fraser and Gawthorpe 2003). This suggests subsidence in the EISB was greater than further south, where the North Wales Platform, which was land attached to the Wales-Brabant Massif, continued to grow. As this subsidence accelerated, isolated carbonate platform growth was maintained on the footwalls of smaller faults, but these platforms started to aggrade as they began to struggle to keep up against the background of regional subsidence.

5.3.3 | Steepening Platform (Mid Visean—Serpukhovian)

From the mid Visean onwards, all the platforms underwent a significant reduction in size relative to their initial platform area, with some platforms having an area almost half of that in the Tournasian (Table 3). There was also a marked steepening in the slope of the platforms from < 15° to > 30° (Figures 10–12). Onshore, sedimentation was terminated across most of the North Wales Platform and the Derbyshire Platform by platform emergence and karstification at the end of the Asbian, after which carbonate growth was re-established, although platforms began to back-step (Davies 2008; Hounslow et al. 2024; Manifold et al. 2021; Somerville and Strank 1984). There was a marked transition from the shallow water grainstone-packstone deposits-often rich in ooids, peloids and corals to the lower energy packstone and wackestone–mudsone facies that were rich in *Gigantoproductius bivalves* and chert (e.g., Somerville and Strank 1984; Marangon et al. 2011). This change in facies suggests that carbonate productivity was increasingly stressed across northern England and Wales, contributing to a consistent backstepping pattern of the platform margins. Similarly, within other carbonate platforms globally (Kenter 1990; Adams and Kenter 2014; Reijmer 2021), slope angles exceeding 30° have been linked to late-stage aggradation, margin backstepping and syn-sedimentary faulting.

The continued reduction of platform size and backstepping of seismic reflectors within the EISB is consistent with this (Figures 10 and 11), particularly with the northern, more distal, areas (A4–6) compared to the larger platforms (e.g., A1, A3) to the south (Figure 8). This suggests that within the study area, subsidence outpaced carbonate accumulation leading to platform drowning (Betzler et al. 2023; Blomeier and Reijmer 2002; Brandano et al. 2015; della Porta et al. 2014). As well as tectonic subsidence, other contributing factors such as changes in relative sea level and ecological stress, likely also contributed to the reduction in carbonate productivity (Betzler et al. 2015; Schlager 1992), but the current dataset does not allow us to resolve these processes in detail.

5.3.4 | Platform Demise (End Mississippian)

By the Serpukhovian, the basin was transitioning into a post-rift thermal subsidence regime, marking a shift in sedimentation dynamics (Fraser and Gawthorpe 2003). Carbonate production was waning, and clastic deposition
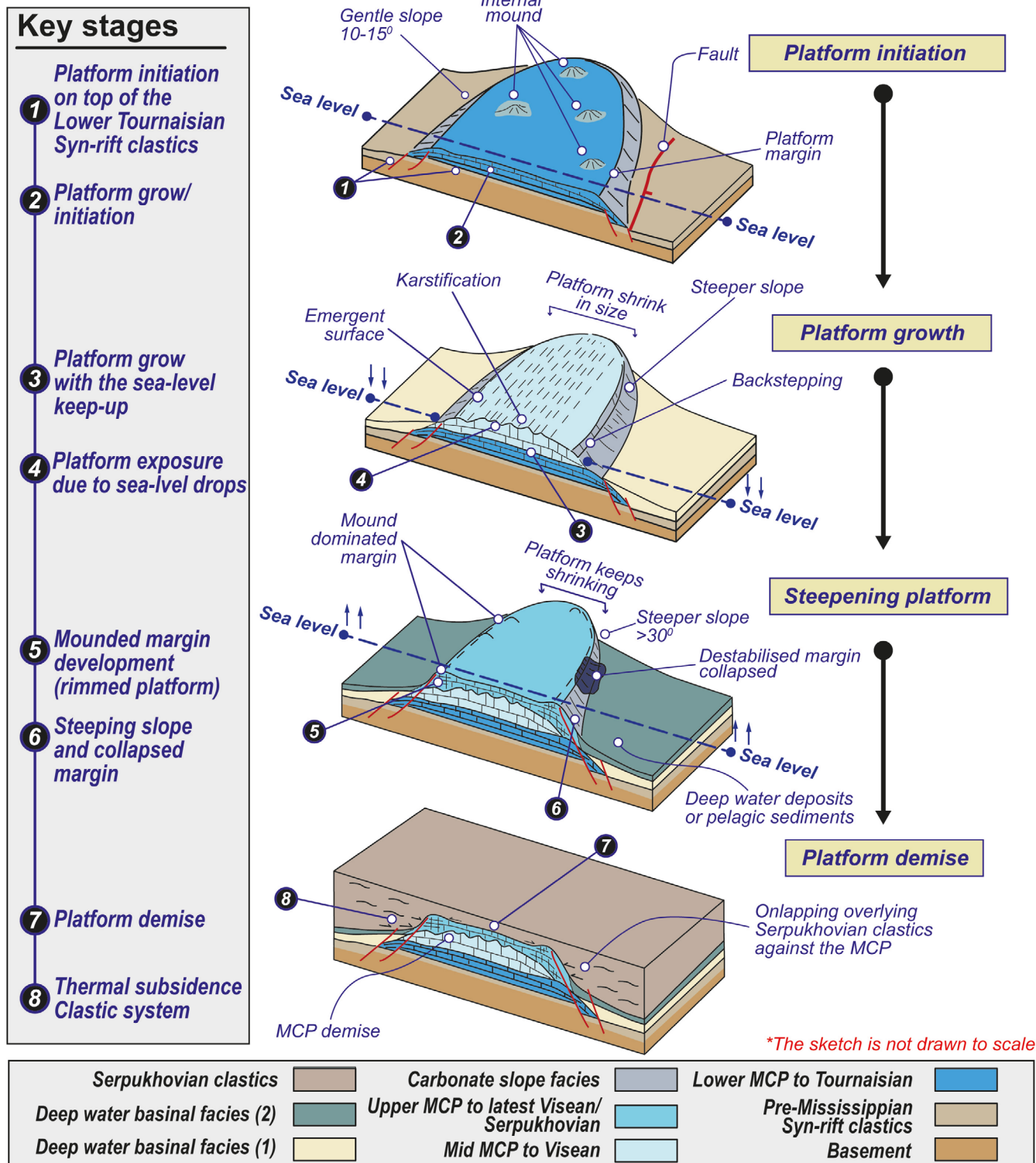
FIGURE 15 | Three-dimensional (3D) evolutionary model of the Mississippian carbonate platform (MCP) in the Irish Sea Basin, illustrating its development from platform initiation in the early Tournaisian to its eventual demise and thermal subsidence. The model highlights the key stages of syn-rift carbonate platform evolution, including initial deposition, growth and subsequent drowning, providing insights into the interplay between tectonic subsidence and carbonate accumulation.

became increasingly dominant, particularly as sediment was sourced from the NW Highlands into northern England (Morton et al. 2024). The increased influx of clastic material during this stage is attributed to enhanced sediment delivery from surrounding landmasses, potentially linked to basin inversion and uplift in adjacent regions (Jackson et al. 1987). Following the demise of carbonate platform growth, seismic data (Figures 5, 6 and 10–12) reveal that these clastic deposits onlap the Mississippian carbonate platforms within the study area as the basin was filled (SF4).

5.4 | Implications

It has long been recognised that carbonate platforms grow preferentially on the footwall of faults during extension, since the elevated topography facilitates carbonate productivity in clear, shallow water (e.g., Bosence 2005; Dorobek 2011). Masiero et al. (2021) modelled controls on carbonate platform architecture and concluded that lateral variability of carbonate platforms is strongly controlled by tectonically controlled differential subsidence. Faulting results in topographic differentiation between footwalls and hanging walls, promoting preferential carbonate platform growth on uplifted footwall blocks within the photic zone. Additionally, faulting generates structural complexity that can influence platform morphology and stability (e.g., Marino and Santantonio 2010).

Carbonate production will keep up with relative sea level rise, even under high rates of subsidence, but excess clastic sediment and/or nutrient ingress into a basin can increase environmental deterioration sufficiently for a carbonate platform to be susceptible to drowning, even without an increase in relative sea level (Van Tuyl et al. 2019; Masiero et al. 2021). During the latest Visean, potentially at the Asbian–Brigantian boundary, there was a transition to global icehouse conditions (Smith and Fred Read 2000; Barnett et al. 2002; Manifold et al. 2021) and it is possible that rapid sea-level rise within an interglacial period led to platform drowning. However, sedimentation on the North Wales Platform remained within shallow water until the Serpukhovian (Manifold et al. 2021). At this point, the onset of thermal subsidence or changing ocean circulation patterns and nutrient flux, associated with clastic influx to the basin, could have all contributed to platform demise. Without the direct observation of facies, it is difficult to determine which of these controls was most important. Overall, however, the cessation of carbonate platform growth and onlap by Pennsylvanian siliciclastic strata is consistent with a transition from shallow-water carbonate sedimentation to deeper-water pelagic and hemipelagic sedimentation.

Importantly, Mississippian carbonate platforms have been recognised as a promising target for deep, low enthalpy, geothermal heat production in the UK and Europe (Busby 2014; Jones et al. 2023; Bos and Laenen 2017; Broothaers et al. 2021; Gutteridge et al. 2025; Mijnlieff 2020). Detailed interpretation of Visean carbonate platforms and their structural configuration in the subsurface of The Netherlands emphasises the role of basement faulting in controlling platform nucleation and evolution (Kombrink et al. 2010; Van Der Voet et al. 2020; van der Voet et al. 2022). Similarly, in the Campine Basin in northern Belgium, structural inheritance, bed thickness and fracture intensity are interpreted as first-order controls on geothermal viability (Swennen et al. 2021). Carbonate platforms in the EISB exhibit comparable structural segmentation and facies variability, especially in the context of fault-controlled growth and steep platform margins (Figure 14). Carbonate platform thickness across the EISB ranges from 1.1 to 2 km, comparable to the maximum thickness observed onshore in NW England (Jones et al. 2023). One of the major challenges in geothermal exploration onshore in the UK is the lack of well penetration and poor onshore seismic imaging, making it difficult to define the geometry and structural complexity of Mississippian carbonate

platforms (Pharaoh et al. 2018). This geological uncertainty increases the risk of resource underperformance, as an incomplete understanding of platform architecture may hinder efficient heat extraction and reservoir sustainability. For example, this study highlights the complex transition of carbonate platforms into adjacent hanging wall basins, with localised carbonate platform growth on small, fault-controlled topographic highs. In an exploration context, this creates a fundamental risk to reservoir presence in the subsurface. Low enthalpy geothermal development requires paired injector-producer wells to be drilled up to 2 km apart, and if one well penetrates a small, isolated carbonate platform then there is a risk that the second well will not encounter carbonate strata, impacting reservoir connectivity and therefore operability.

An additional risk is the depth of the carbonate platforms, which varies significantly across the study area, ranging from 1 to 3 km (Figure 8). This depth variation has a direct impact on heat in place, with deeper platforms providing higher heat potential but also posing greater exploration risks due to seismic data quality. The porosity and permeability of the carbonate platforms are also critical uncertainties. Seismic facies analysis indicates the possibility of karstified intervals, recognised as disrupted seismic reflections (~70 ms TWT, ~170 m thick), which could significantly influence fluid flow properties and heat transfer efficiency. While karstification can enhance reservoir permeability by increasing secondary porosity (Moore and Walsh 2021), it can also create heterogeneous flow pathways that lead to uneven heat extraction rates and potential reservoir compartmentalization (Narayan et al. 2021).

Structural controls, particularly fault properties and fracture permeability, play an equally important role in defining the geothermal potential of the carbonate platforms (Elvebakk et al. 2002). Seismic interpretation reveals that faults within the carbonate interval display a wide range of displacements, from small to major offsets (Figure 9a,b), with the majority exhibiting a north–south (N-S) orientation. These fault systems likely reflect multiple tectonic episodes, including early Devonian extension to Mississippian extension, Pennsylvanian subsidence and Variscan tectonic reactivation (Pickard et al. 1994; Smit et al. 2018). Understanding the distribution of these faults, and the permeability of faults and fractures, is critical for predicting reservoir behaviour, as they may act as either high-permeability conduits that enhance heat extraction or sealing barriers that compartmentalise fluid flow (Lipsey et al. 2015).

6 | Conclusions

This study provides a comprehensive analysis of the transition of the North Wales Platform into the East Irish Sea Basin (EISB), demonstrating that instead of a simple platform-to-basin transition, there exists a complex configuration of numerous smaller, fault-controlled carbonate platforms. These findings enhance our understanding of the depositional and tectonic processes that governed the platform to basin transition and demonstrate that carbonate growth persisted on structural highs within the basin, as smaller, isolated carbonate platforms that back-stepped and drowned in the late Visean. Overall, the occurrence and size of Mississippian carbonate platforms in the EISB exhibit greater

complexity than anticipated from regional tectonostratigraphic models. The carbonate platforms are distributed across six distinct areas (A1–A6), each characterised by unique geometries and irregular morphologies extending approximately 40 km northward. Platform thicknesses range from 0.5 to 2 km, with the thickest sections (1.1–2 km) concentrated in the southern domain. Platform demise is evident first in the northern domain, where the top of the Mississippian is at ~3.5 km, with a platform thickness of < 1 km.

Syn-sedimentary faulting played a crucial role in shaping the occurrence of carbonate platforms in the EISB. This is indicated by the EI values (< 1), which suggest active faulting during carbonate growth and development. Faults exhibit a wide range of throws, from small displacements influencing the top of the Mississippian to major faults that significantly impact basin morphology. Thickening of Mississippian strata in the footwall, observed in this study, supports the role of fault-controlled carbonate growth in the region. The dominant north–south trend of the faults is inconsistent with the regional N-S oriented extension direction, and most likely reflects inheritance of the precursor structural grain in the basin.

The internal geometry of the carbonate platforms indicates platform initiation in the Tournaisian with a relatively low angle platform slope, which progressively steepened to 30°–35° in the Visean, with backstepping evident in late Visean strata. This steepening, coupled with increasing subsidence, resulted in a shrinkage of the platform by up to 49% from its initial size between the Tournaisian and Visean indicating progressive drowning of the carbonate platforms as the basin moved into thermal subsidence from the Pennsylvanian.

Despite challenges associated with variable seismic data quality, this study demonstrates that meaningful geological interpretation can be achieved through the integration of carbonate platform development concepts, regional geological context and a systematic seismic facies workflow. These combined approaches allowed robust characterisation of seismic architectures and facies distributions, leading to new insights into Mississippian carbonate platform evolution in the EISB. These findings hold significant implications for geothermal exploration, particularly in assessing the presence, size and spatial complexity of Mississippian carbonate platforms. The variability in platform distribution and orientation provides critical insights for optimising future onshore data acquisition and targeting potential geothermal reservoirs. Key geological features that might influence geothermal potential include steep platform slopes, collapsed margins within the Visean strata and evidence of karstified intervals in intra-Visean sequences. These characteristics directly impact the feasibility of geothermal energy extraction, as they influence reservoir quality, permeability and fluid flow dynamics within Mississippian carbonate platforms.

Conflicts of Interest

The authors declare no conflicts of interest.

Data Availability Statement

The authors have nothing to report.

References

Adams, A. E., A. D. Horbury, and A. A. Abdel Aziz. 1990. "Controls on Dinantian Sedimentation in South Cumbria and Surrounding Areas of Northwest England." *Proceedings of the Geologists' Association* 101, no. 1: 19–30. https://doi.org/10.1016/S0016-7878(08)80203-9.

Adams, A. E. W., and J. A. M. Kenter. 2014. "So Different, Yet So Similar: Comparing and Contrasting Siliciclastic and Carbonate Slopes." In *Deposits, Architecture, and Controls of Carbonate Margin, Slope, and Basinal Settings*, 14–25. SEPM (Society for Sedimentary Geology). https://doi.org/10.2110/sepmsp.105.14.

Armstrong, P., C. Durrand, I. Barany, and T. Butaud. 2004. "Seismic Measurements While Drilling Reduce Uncertainty in the Deepwater Gulf of Mexico." *SEG Technical Program Expanded Abstracts* 23, no. 1: 2470–2473. https://doi.org/10.1190/1.1851248.

Bachtel, S. L., R. D. Kissling, D. Martono, S. P. Rahardjanto, P. A. Dunn, and B. A. MacDonald. 2005. *Seismic Stratigraphic Evolution of the Miocene-Pliocene Segitiga Platform, East Natuna Sea, Indonesia: The Origin, Growth, and Demise of an Isolated Carbonate Platform*, 81. AAPG Memoir.

Badali, M. 2024. "Seismic Expression of Shallow-Water Carbonate Structures Through Geologic Time." *Interpretation* 12, no. 2: T119–T147. https://doi.org/10.1190/INT-2023-0014.1.

Barnaby, R. J., and J. F. Read. 1990. "Carbonate Ramp to Rimmed Shelf Evolution: Lower to Middle Cambrian Continental Margin, Virginia Appalachians." *Bulletin of the Geological Society of America* 102, no. 3: 391–404. https://doi.org/10.1130/0016-7606(1990)102<0391:CRTRSE>2.3.CO;2.

Barnett, A. J., P. M. Burgess, and V. P. Wright. 2002. "Icehouse World Sea-Level Behaviour and Resulting Stratal Patterns in Late Visean (Mississippian) Carbonate Platforms: Integration of Numerical Forward Modelling and Outcrop Studies." *Basin Research* 14, no. 3: 417–438. https://doi.org/10.1046/j.1365-2117.2002.00186.x.

Bashir, Y., M. A. Faisal, A. Biswas, et al. 2021. "Seismic Expression of Miocene Carbonate Platform and Reservoir Characterization Through Geophysical Approach: Application in Central Luconia, Offshore Malaysia." *Journal of Petroleum Exploration and Production* 11, no. 4: 1533–1544. https://doi.org/10.1007/s13202-021-01132-2.

Betzler, C., S. Lindhorst, T. Lüdmann, B. Weiss, M. Wunsch, and J. C. Braga. 2015. "The Leaking Bucket of a Maldives Atoll: Implications for the Understanding of Carbonate Platform Drowning." *Marine Geology* 366: 16–33. https://doi.org/10.1016/j.margeo.2015.04.009.

Betzler, C., S. Lindhorst, J. J. G. Reijmer, et al. 2023. "Carbonate Platform Drowning Caught in the Act: The Sedimentology of Saya de Malha Bank (Indian Ocean)." *Sedimentology* 70, no. 1: 78–99. https://doi.org/10.1111/sed.13032.

Blomeier, D. P. G., and J. J. G. Reijmer. 2002. "Facies Architecture of an Early Jurassic Carbonate Platform Slope (Jbel Bou Dahar, High Atlas, Morocco)." *Journal of Sedimentary Research* 72, no. 4: 462–475. https://doi.org/10.1306/111501720462.

Bos, S., and B. Laenen. 2017. "Development of the First Deep Geothermal Doublet in the Campine Basin of Belgium." *European Geologist Journal* 43: 16–20.

Bosence, D. 2005. "A Genetic Classification of Carbonate Platforms Based on Their Basinal and Tectonic Settings in the Cenozoic." *Sedimentary Geology* 175: 49–72. https://doi.org/10.1016/j.sedgeo.2004.12.030.

Brandano, M., M. Lustrino, I. Cornacchia, and M. Sprovieri. 2015. "Global and Regional Factors Responsible for the Drowning of the Central Apennine Chattian Carbonate Platforms." *Geological Journal* 50, no. 5: 575–591. https://doi.org/10.1002/gj.2575.

Broothaers, M., D. Lagrou, B. Laenen, V. Harcouët-Menou, and D. Vos. 2021. "Deep Geothermal Energy in the Lower Carboniferous Carbonates of the Campine Basin, Northern Belgium: An Overview From the 1950's to 2020." *Zeitschrift der Deutschen Gesellschaft für Geowissenschaften* 172, no. 3: 211. https://doi.org/10.1127/zdgg/2021/0285.

Burchette, T. P., and V. P. Wright. 1992. "Carbonate Ramp Depositional Systems." *Sedimentary Geology* 79, no. 1–4: 3–57. https://doi.org/10.1016/0037-0738(92)90003-A.

Burgess, P. M., P. Winefield, M. Minzoni, and C. Elders. 2013. "Methods for Identification of Isolated Carbonate Buildups From Seismic Reflection Data." *AAPG Bulletin* 97, no. 7: 1071–1098. https://doi.org/10.1306/12051212011.

Busby, J. 2014. "Geothermal Energy in Sedimentary Basins in the UK." *Hydrogeology Journal* 22, no. 1: 129–141. https://doi.org/10.1007/s10040-013-1054-4.

Cartwright, J., B. Trudgill, and C. Mansfield. 2000. "Fault Growth by Segment Linkage: An Explanation for Scatter in Maximum Displacement and Trace Length Data From the Canyonlands Grabens of SE Utah: Reply Journal of Structural Geology (22, 1)." *Journal of Structural Geology* 22, no. 1: 1319. https://doi.org/10.1016/S0191-8141(99)00135-2.

Cartwright, J. A., C. Mansfield, and B. Trudgill. 1996. "The Growth of Normal Faults by Segment Linkage." *Geological Society Special Publication* 99: 163–177. https://doi.org/10.1144/GSL.SP.1996.099.01.13.

Chadwick, R. A., and D. J. Evans. 1995. "The Timing and Direction of Permo-Triassic Extension in Southern Britain." *Geological Society Special Publication* 91: 161–192. https://doi.org/10.1144/GSL.SP.1995.091.01.09.

Chadwick, R. A., D. J. Evans, and D. W. Holliday. 1993. "The Maryport Fault: The Post-Caledonian Tectonic History of Southern Britain in Microcosm." *Journal of the Geological Society of London* 150, no. 2: 247–250. https://doi.org/10.1144/gsjgs.150.2.0247.

Chee, O. P., M. Poppelreiter, D. Ghosh, R. Lazar, and U. Djuraev. 2018. "Study of a TX Field Miocene Carbonate Build-Up: Integration of Sedimentological Data With Modern Carbonate Analogue and 3D Seismic Characterization to Establish Carbonate Facies Modelling Workflow." *Bulletin-Geological Society of Malaysia* 65: 135–140. https://doi.org/10.7186/bgsm65201816.

Corfield, S. M., R. L. Gawthorpe, M. Gage, A. J. Fraser, and B. M. Besly. 1996. "Inversion Tectonics of the Variscan Foreland of the British Isles." *Journal of the Geological Society* 153, no. 1: 17–32. https://doi.org/10.1144/gsjgs.153.1.0017.

Couleou, T. 2020. "On the Use of Seismic Velocities in Model Building for Depth Conversion." https://doi.org/10.3997/2214-4609-pdb.15.iv-1.

Coward, M. P. 1993. "The Effect of Late Caledonian and Variscan Continental Escape Tectonics on Basement Structure, Paleozoic Basin Kinematics and Subsequent Mesozoic Basin Development in NW Europe." *Petroleum Geology Conference Proceedings* 4: 1095–1108. https://doi.org/10.1144/0041095.

Coward, M. P. 1995. "Structural and Tectonic Setting of the Permo-Triassic Basins of Northwest Europe." *Geological Society Special Publication* 91: 7–39. https://doi.org/10.1144/GSL.SP.1995.091.01.02.

Davies, S. J. 2008. "The Record of Carboniferous Sea-Level Change in Low-Latitude Sedimentary Successions From Britain and Ireland During the Onset of the Late Paleozoic Ice Age." *Special Paper of the Geological Society of America* 441: 187–20410. https://doi.org/10.1130/2008.2441(13).

de Jonge-Anderson, I., and J. R. Underhill. 2020. "Structural Constraints on Lower Carboniferous Shale Gas Exploration in the Craven Basin, NW England." *Petroleum Geoscience* 26, no. 2: 303–324. https://doi.org/10.1144/petgeo2019-125.

del Strother, P., A. Giże, C. Hollis, and D. McLean. 2021. "Bituminous Coals on Emergent Surfaces in an Asbian, Lower Carboniferous (Mississippian) Limestone Succession on the North Wales Carbonate Platform, UK, and Implications for Palaeoclimate." *Proceedings of the Yorkshire Geological Society* 63, no. 4: pygs2020-006.63. https://doi.org/10.1144/pygs2020-006.

Della Porta, G., J. A. M. Kenter, and J. R. Bahamonde. 2004. "Depositional Facies and Stratal Geometry of an Upper Carboniferous Prograding and Aggrading High-Relief Carbonate Platform (Cantabrian Mountains, N Spain)." *Sedimentology* 51, no. 2: 267–295. https://doi.org/10.1046/j.1365-3091.2003.00621.x.

della Porta, G., O. Merino-Tomé, J. A. M. Kenter, and K. Verwer. 2014. "Lower Jurassic Microbial and Skeletal Carbonate Factories and Platform Geometry (Djebel Bou Dahar, High Atlas, Morocco)." In *Deposits, Architecture, and Controls of Carbonate Margin, Slope, and Basinal Settings*, 237–263. SEPM (Society for Sedimentary Geology). https://doi.org/10.2110/sepmsp.105.01.

Deraisme, J., and N. Jeannee. 2020. "Quantifying Uncertainty in Depth Conversion and Volumetrics." https://doi.org/10.3997/2214-4609-pdb.8.t001.

Dorobek, S. L. 2011. "Tectonic and Depositional Controls on Syn-Rift Carbonate Platform Sedimentation." In *Controls on Carbonate Platform and Reef Development*, 57–81. SEPM (Society for Sedimentary Geology). https://doi.org/10.2110/pec.08.89.0057.

Duffy, O. B., R. E. Bell, C. A. L. Jackson, R. L. Gawthorpe, and P. S. Whipp. 2015. "Fault Growth and Interactions in a Multiphase Rift Fault Network: Horda Platform, Norwegian North Sea." *Journal of Structural Geology* 80: 99–119. https://doi.org/10.1016/j.jsg.2015.08.015.

Ebdon, C. C., A. J. Fraser, A. C. Higgins, B. C. Mitchener, and A. R. E. Strank. 1990. "The Dinantian Stratigraphy of the East Midlands: A Seismostratigraphic Approach." *Journal of the Geological Society of London* 147, no. 3: 519–536. https://doi.org/10.1144/gsjgs.147.3.0519.

Eberli, G. P., and C. Betzler. 2019. "Characteristics of Modern Carbonate Contourite Drifts." *Sedimentology* 66, no. 4: 1163–1191. https://doi.org/10.1111/sed.12584.

Elam, S. D., J. Beall, and C. Wood. 2020. "Depth Conversion and Uncertainty of Depth Migrated Seismic From the Southern North Sea." https://doi.org/10.3997/2214-4609-pdb.5.f015.

Elvebakk, G., D. W. Hunt, and L. Stemmerik. 2002. "From Isolated Buildups to Buildup Mosaics: 3D Seismic Sheds New Light on Upper Carboniferous-Permian Fault Controlled Carbonate Buildups, Norwegian Barents Sea." *Sedimentary Geology* 152, no. 1-2: 7–17. https://doi.org/10.1016/S0037-0738(02)00232-4.

Embry, J. C., D. W. Hunt, A. Colpaert, A. Dræge, and L. Zahm. 2021. "Seismic Facies, Stratigraphy, Geomorphology, and Seismic Modelling of a Lower Cretaceous Carbonate Platform." *GeoPlogical Society Special Publication* 509, no. 1: SP509-2020-18. https://doi.org/10.1144/SP509-2020-18.

EMODnet Bathymetry Consortium. 2022. "EMODnet Digital Bathymetry (DTM)–2022 Release." Https://Www.Emodnet-Bathymetry.Eu.

Etienne, S., P. Le Roy, E. Tournadour, et al. 2021. "Large-Scale Margin Collapses Along a Partly Drowned, Isolated Carbonate Platform (Lansdowne Bank, SW Pacific Ocean)." *Marine Geology* 436: 106477. https://doi.org/10.1016/j.margeo.2021.106477.

Fraser, A. J., and R. L. Gawthorpe. 1990. "Tectono-Stratigraphic Development and Hydrocarbon Habitat of the Carboniferous in Northern England." *Geological Society Special Publication* 55: 49–86. https://doi.org/10.1144/GSL.SP.1990.055.01.03.

Fraser, A. J., and R. L. Gawthorpe. 2003. "An Atlas of Carboniferous Basin Evolution in Northern England." *Marine and Petroleum Geology* 21, no. 3: 421. https://doi.org/10.1016/j.marpetgeo.2004.02.001.

Fraser, A. J., D. F. Nash, R. P. Steele, and C. C. Ebdon. 1990. "A Regional Assessment of the Intra-Carboniferous Play of Northern England." *Geological Society Special Publication* 50: 417–440. https://doi.org/10.1144/GSL.SP.1990.050.01.26.

Fyhn, M. B. W., L. O. Boldreel, L. H. Nielsen, et al. 2013. "Carbonate Platform Growth and Demise Offshore Central Vietnam: Effects of Early Miocene Transgression and Subsequent Onshore Uplift." *Journal of Asian Earth Sciences* 76: 152–168. https://doi.org/10.1016/j.jseaes.2013.02.023.

Gamboa, D., J. D. O. Williams, M. Bentham, D. I. Schofield, and A. C. Mitchell. 2019. "Application of Three-Dimensional Fault Stress Models for Assessment of Fault Stability for CO2 Storage Sites." *International Journal of Greenhouse Gas Control* 90: 102820. https://doi.org/10.1016/j.ijggc.2019.102820.

Gawthorpe, R. 1986. "Sedimentation During Carbonate Ramp-to-Slope Evolution in a Tectonically Active Area: Bowland Basin (Dinantian), Northern England." *Sedimentology* 33, no. 2: 185–206. https://doi.org/10.1111/j.1365-3091.1986.tb00531.x.

Gómez-Pérez, I., P. A. Fernández-Mendiola, and J. García-Mondéjar. 1999. "Depositional Architecture of a Rimmed Carbonate Platform (Albian, Gorbea, Western Pyrenees)." *Sedimentology* 46, no. 2: 337–356. https://doi.org/10.1046/j.1365-3091.1999.00217.x.

Gutteridge, P. 2024. "Lacustrine and Palustrine Carbonates in a Brigantian (Late Dinantian) Intrashelf Basin in the Derbyshire Carbonate Platform." *Geological Journal* 59, no. 3: 951–964. https://doi.org/10.1002/gj.4901.

Gutteridge, P., J. Ten Veen, J. Dewit, et al. 2025. "Regional Assessment of the Ultra-Deep Geothermal (UDG) Reservoir Quality and Potential of the Dinantian Zeeland Formation, the Netherlands." *Geological Society, London, Special Publications* 548, no. 1: 267–290. https://doi.org/10.1144/sp548-2023-106.

Hendry, J., P. Burgess, D. Hunt, et al. 2021. "Seismic Characterization of Carbonate Platforms and Reservoirs: An Introduction and Review." *Geological Society Special Publication* 509, no. 1: 1–28. https://doi.org/10.1144/SP509-2021-51.

Hounslow, M. W., P. Cózar, I. D. Somerville, and A. J. Biggin. 2024. "Rock Magnetic-Based Cyclic Expression in Late Visean Ramp Carbonates and an Astrochronology for the Late Asbian From Northwest England."

Paleoceanography and Paleoclimatology 39, no. 3: e2023PA004772. https://doi.org/10.1029/2023PA004772.

Hu, X., W. Zheng, X. Zhao, and B. Niu. 2023. "Quantitative Characterization of Deep Fault-Karst Carbonate Reservoirs: A Case Study of the Yuejin Block in the Tahe Oilfield." *Energy Geoscience* 4, no. 3: 100153. https://doi.org/10.1016/j.engeos.2022.100153.

Jackson, C. A. L., R. E. Bell, A. Rotevatn, and A. B. M. Tvedt. 2017. "Techniques to Determine the Kinematics of Synsedimentary Normal Faults and Implications for Fault Growth Models." *Geological Society Special Publication* 439, no. 1: 187–217. https://doi.org/10.1144/SP439.22.

Jackson, C. A. L., and A. Rotevatn. 2013. "3D Seismic Analysis of the Structure and Evolution of a Salt-Influenced Normal Fault Zone: A Test of Competing Fault Growth Models." *Journal of Structural Geology* 54: 215–234. https://doi.org/10.1016/j.jsg.2013.06.012.

Jackson, D. I., A. A. Jackson, D. Evans, R. T. R. Wingfield, R. P. Barnes, and M. J. Arthur. 1995. *United Kingdom Offshore Regional Report: The Geology of the Irish Sea*. HMSO for the British Geological Survey.

Jackson, D. I., H. Johnson, and N. J. P. Smith. 1997. "Stratigraphical Relationships and a Revised Lithostratigraphical Nomenclature for the Carboniferous, Permian and Triassic Rocks of the Offshore East Irish Sea Basin." *Geological Society Special Publication* 124: 11–32. https://doi.org/10.1144/GSL.SP.1997.124.01.02.

Jackson, D. I., N. S. Jones, and C. N. Waters. 2011. "A Revised Correlation of Carboniferous Rocks in the British Isles." *Geological Society* 26: 110–116. https://doi.org/10.1144/SR26.16.

Jackson, D. I., and P. Mulholland. 1993. "Tectonic and Stratigraphic Aspects of the East Irish Sea Basin and Adjacent Areas: Contrasts in Their Post-Carboniferous Structural Styles." *Petroleum Geology Conference Proceedings* 4: 791–808. https://doi.org/10.1144/0040791.

Jackson, D. I., P. Mulholland, S. M. Jones, and G. Warrington. 1987. "Proceedings 3rd Conference London." In *The Geological Framework of the East Irish Sea Basin. Petroleum Geology of North West Europe*, vol. 1. Graham & Trotman Limited.

Jiménez Berrocoso, Á., M. Masini, J. Salazar, A. O. Campos, and J. C. C. Hsieh. 2021. "Challenges of Carbonate Platform Identification and Characterization From Seismic Data in Frontier Exploration–Evaluating a Possible Miocene Example From the SE Caribbean." *Geological Society, London, Special Publications* 509, no. 1: 57–88. https://doi.org/10.1144/SP509-2019-200.

Jones, D. J. R., T. Randles, T. Kearsey, T. C. Pharaoh, and A. Newell. 2023. "Deep Geothermal Resource Assessment of Early Carboniferous Limestones for Central and Southern Great Britain." *Geothermics* 109: 102649. https://doi.org/10.1016/j.geothermics.2023.102649.

Juerges, A., C. E. Hollis, J. Marshall, and S. Crowley. 2016. "The Control of Basin Evolution on Patterns of Sedimentation and Diagenesis: An Example From the Mississippian Great Orme, North Wales." *Journal of the Geological Society* 173, no. 3: 438–456. https://doi.org/10.1144/jgs2014-149.

Jutras, P., J. McLeod, R. A. MacRae, and J. Utting. 2016. "Complex Interplay of Faulting, Glacioeustatic Variations and Halokinesis During Deposition of Upper Viséan Units Over Thick Salt in the Western Cumberland Basin of Atlantic Canada." *Basin Research* 28, no. 4: 483–506. https://doi.org/10.1111/bre.12119.

Kenter, J. A. M. 1990. "Carbonate Platform Flanks: Slope Angle and Sediment Fabric." *Sedimentology* 37, no. 5: 777–794. https://doi.org/10.1111/j.1365-3091.1990.tb01825.x.

Kirkham, A. 2021. "Mass Collapse and Resedimentation on a Brigantian–Early Namurian Platform Margin, Halkyn–Mold Area, North Wales, UK." *Geological Journal* 56, no. 7: 3672–3686. https://doi.org/10.1002/gj.4127.

Knipe, R. J., G. Cowan, and V. S. Balendran. 1993. "The Tectonic History of the East Irish Sea Basin With Reference to the Morecambe

Fields." *Petroleum Geology Conference Proceedings* 4: 857–866. https://doi.org/10.1144/0040857.

Koehl, J. B. P., G. Christophersen, M. Collombin, C. Taule, E. M. B. Stokmo, and L. Allaart. 2023. "Devonian-Mississippian Faulting Controlled by WNW-ESE-Striking Structural Grain in Proterozoic Basement Rocks in Billefjorden, Central Spitsbergen." *Geologica Acta* 21: 1–16. https://doi.org/10.1344/GeologicaActa2023.21.7.

Kombrink, H., H. van Lochem, and K. J. Zwan. 2010. "Seismic Interpretation of Dinantian Carbonate Platforms in the Netherlands; Implications for the Palaeogeographical and Structural Development of the Northwest European Carboniferous Basin." *Journal of the Geological Society* 167, no. 1: 99–108. https://doi.org/10.1144/0016-76492008-149.

Kremor, J., M. Agarwal, P. Spaans, and U. S. Wong. 2019. "Depth Conversion and Seismic Inversion of the Scarborough Gas Field." *Exploration Geophysics* 2019, no. 1: 1–4. https://doi.org/10.1080/22020586.2019.12072991.

Leeder, M. R., and R. L. Gawthorpe. 1987. "Sedimentary Models for Extensional Tilt-Block/Half- Graben Basins." *Continental Extensional Tectonics* 28: 139–152.

Lipsey, L. C., J. D. van Wees, and M. P. D. Pluymaekers. 2015. "First EAGE/TNO Workshop." In *Numerical Modelling of Thermal Convection Related to Fracture Permeability-Implications for Geothermal Exploration and Basin Modelling.* Harvard. https://doi.org/10.3997/2214-4609.201412330.

Loza Espejel, R., T. M. Alves, and T. G. Blenkinsop. 2019. "Distribution and Growth Styles of Isolated Carbonate Platforms as a Function of Fault Propagation." *Marine and Petroleum Geology* 107: 484–507. https://doi.org/10.1016/j.marpetgeo.2019.05.020.

Lucas, S. G., J. W. Schneider, S. Nikolaeva, and X. Wang. 2022. "The Carboniferous Timescale: An Introduction." *Geological Society Special Publication* 512, no. 1: 1–17. https://doi.org/10.1144/SP512-2021-160.

Lukasik, J., and J. Simo. 2008. "Controls on Carbonate Platform and Reef Development." In *Controls on Carbonate Platform and Reef Development.* SEPM Society for Sedimentary Geology. https://doi.org/10.2110/pec.08.89.

Makhankova, A., B. Sautter, M. Mathew, D. Menier, and M. Poppelreiter. 2021. "Seismic Stratigraphy and Sedimentology of a Miocene Carbonate Platform in Luconia, South China Sea." *Geological Journal* 56, no. 1: 1–17. https://doi.org/10.1002/gj.3942.

Manifold, L., P. Del Strother, D. P. Gold, P. Burgess, and C. Hollis. 2021. "Unravelling Evidence for Global Climate Change in Mississippian Carbonate Strata From the Derbyshire and North Wales Platforms, UK." *Journal of the Geological Society* 178, no. 5: jgs2020-106. https://doi.org/10.1144/jgs2020-106.

Manifold, L., C. Hollis, and P. Burgess. 2020. "The Anatomy of a Mississippian (Viséan) Carbonate Platform Interior, UK: Depositional Cycles, Glacioeustasy and Facies Mosaics." *Sedimentary Geology* 401: 105633. https://doi.org/10.1016/j.sedgeo.2020.105633.

Marangon, A., G. Gattolin, G. Della Porta, and N. Preto. 2011. "The Latemar: A Flat-Topped, Steep Fronted Platform Dominated by Microbialites and Synsedimentary Cements." *Sedimentary Geology* 240, no. 3–4: 97–114. https://doi.org/10.1016/j.sedgeo.2011.09.001.

Marino, M., and M. Santantonio. 2010. "Understanding the Geological Record of Carbonate Platform Drowning Across Rifted Tethyan Margins: Examples From the Lower Jurassic of the Apennines and Sicily (Italy)." *Sedimentary Geology* 225, no. 3–4: 116–137. https://doi.org/10.1016/j.sedgeo.2010.02.002.

Masaferro, J. L., R. Bourne, and J. C. Jauffred. 2005. *Three-Dimensional Seismic Volume Visualization of Carbonate Reservoirs and Structures.* Vol. 81, 11–41. AAPG Memoir.

Masiero, I., P. Burgess, C. Hollis, et al. 2021. "Syn-Rift Carbonate Platforms in Space and Time: Testing and Refining Conceptual Models Using Stratigraphic and Seismic Numerical Forward Modelling." *Geological Society Special Publication* 509, no. 1: 179–203. https://doi.org/10.1144/SP509-2019-217.

Mijnlieff, H. F. 2020. "Introduction to the Geothermal Play and Reservoir Geology of the Netherlands." *Netherlands Journal of Geosciences* 99: e2. https://doi.org/10.1017/njg.2020.2.

Moore, J. P., and J. J. Walsh. 2021. "Quantitative Analysis of Cenozoic Faults and Fractures and Their Impact on Groundwater Flow in the Bedrock Aquifers of Ireland." *Hydrogeology Journal* 29, no. 8: 2613–2632. https://doi.org/10.1007/s10040-021-02395-z.

Morton, A. C., J. I. Chisholm, and D. Frei. 2024. "Provenance Response to Evolving Palaeogeography Recorded by Carboniferous Sandstones in the Northern Pennine Basin, UK." *Sedimentary Geology* 470: 106691. https://doi.org/10.1016/j.sedgeo.2024.106691.

Mundy, D. J. C. 1992. "Microbialite-Sponge-Bryozoan-Coral Framestones in Lower Carboniferous (Late Visean) Buildups of Northern England (UK)." *Canadian Society of Petroleum Geologists* 17: 713–729.

Narayan, N. S., C. A. Adams, and J. G. Gluyas. 2021. "Karstified and Fractured Lower Carboniferous (Mississippian) Limestones of the UK – A Cryptic Geothermal Reservoir." *Zeitschrift der Deutschen Gesellschaft für Geowissenschaften* 172, no. 3: 251–265. https://doi.org/10.1127/zdgg/2021/0288.

Needham, T., and R. Morgan. 1997. "The East Irish Sea and Adjacent Basins: New Faults or Old?" *Journal of the Geological Society* 154, no. 1: 145–150. https://doi.org/10.1144/gsjgs.154.1.0145.

Paumard, V., E. Zuckmeyer, R. Boichard, et al. 2017. "Evolution of Late Oligocene - Early Miocene Attached and Isolated Carbonate Platforms in a Volcanic Ridge Context (Maldives Type), Yadana Field, Offshore Myanmar." *Marine and Petroleum Geology* 81: 361–387. https://doi.org/10.1016/j.marpetgeo.2016.12.012.

Peacock, D. C. P., D. J. Sanderson, and A. Rotevatn. 2018. "Relationships Between Fractures." *Journal of Structural Geology* 106: 41–53. https://doi.org/10.1016/j.jsg.2017.11.010.

Pharaoh, K., M. Kirk, M. Quinn, M. Sankey, and A. A. Monaghan. 2016. "Energy and Marine Geoscience Programme Commissioned Report." In *Seismic Interpretation and Generation of Depth Surfaces for Late Palaeozoic Strata in the Irish Sea Region*, 65. Natural Environment Research Council.

Pharaoh, T., R. Haslam, E. Hough, et al. 2020. "The Môn-Deemster-Ribblesdale Fold-Thrust Belt, Central UK: A Concealed Variscan Inversion Belt Located on Weak Caledonian Crust." *Geological Society Special Publication* 490, no. 1: 153–176. https://doi.org/10.1144/SP490-2018-109.

Pharaoh, T., D. Jones, T. Kearsey, et al. 2021. "Early Carboniferous Limestones of Southern and Central Britain: Characterisation and Preliminary Assessment of Deep Geothermal Prospectivity." *Zeitschrift der Deutschen Gesellschaft für Geowissenschaften* 172, no. 3: 227–249. https://doi.org/10.1127/zdgg/2021/0282.

Pharaoh, T., N. J. P. Smith, K. Kirk, et al. 2016. *Palaeozoic Petroleum Systems of the Irish Sea.* British Geological Survey.

Pharaoh, T. C., C. M. A. Gent, S. D. Hannis, et al. 2018. "An Overlooked Play? Structure, Stratigraphy and Hydrocarbon Prospectivity of the Carboniferous in the East Irish Sea-North Channel Basin Complex." *Geological Society Special Publication* 471, no. 1: 281–316. https://doi.org/10.1144/SP471.7.

Phillips, E., D. M. Hodgson, and A. R. Emery. 2017. "The Quaternary Geology of the North Sea Basin." *Journal of Quaternary Science* 32, no. 2: 117–126. https://doi.org/10.1002/jqs.2932.

Pickard, N. A. H., J. G. Rees, P. Strogen, I. D. Somerville, and G. L. I. Jones. 1994. "Controls on the Evolution and Demise of Lower Carboniferous Carbonate Platforms, Northern Margin of the Dublin

Basin, Ireland." *Geological Journal* 29, no. 2: 93–117. https://doi.org/10.1002/gj.3350290202.

Pomar, L. 2001. "Types of Carbonate Platforms: A Genetic Approach." *Basin Research* 13, no. 3: 313–334. https://doi.org/10.1046/j.0950-091X.2001.00152.x.

Quirk, D. G., and G. S. Kimbell. 1997. "Structural Evolution of the Isle of Man and Central Part of the Irish Sea." *Geological Society Special Publication* 124: 135–159. https://doi.org/10.1144/GSL.SP.1997.124.01.09.

Reijmer, J. J. G. 2021. "Marine Carbonate Factories: Review and Update." *Sedimentology* 68, no. 5: 1729–1796. https://doi.org/10.1111/sed.12878.

Reijmer, J. J. G., J. H. Ten Veen, B. Jaarsma, and R. Boots. 2017. "Seismic Stratigraphy of Dinantian Carbonates in the Southern Netherlands and Northern Belgium." *Netherlands Journal of Geosciences* 96, no. 4: 353–379. https://doi.org/10.1017/njg.2017.33.

Schlager, W. 1992. "Sedimentology and Sequence Stratigraphy of Reefs and Carbonate Platforms." https://doi.org/10.1016/0264-8172(94)90087-6.

Schofield, D. I., A. G. Leslie, P. R. Wilby, R. Dartnall, J. W. F. Waldron, and R. S. Kendall. 2021. "Tectonic Evolution of Anglesey and Adjacent Mainland North Wales." In *Geological Society Special Publication* (Vol. 503, no. 1). https://doi.org/10.1144/SP503-2020-9.

Schofield, K., and A. E. Adams. 1985. "Stratigraphy and Depositional Environments of the Woo Dale Limestones Formation (Dinantian), Derbyshire." *Proceedings of the Yorkshire Geological Society* 45, no. 4: 225–233. https://doi.org/10.1144/pygs.45.4.225.

Smit, J., J. D. van Wees, and S. Cloetingh. 2018. "Early Carboniferous Extension in East Avalonia: 350 My Record of Lithospheric Memory." *Marine and Petroleum Geology* 92: 1010–1027. https://doi.org/10.1016/j.marpetgeo.2018.01.004.

Smith, L. B., and J. Fred Read. 2000. "Rapid Onset of Late Paleozoic Glaciation on Gondwana: Evidence From Upper Mississippian Strata of the Midcontinent, United States." *Geology* 28, no. 3: 279. https://doi.org/10.1130/0091-7613(2000)28<>2.0.CO;2.

Somerville, I. D. 2003. *Review of Irish Lower Carboniferous (Mississippian) Mud Mounds; Depositional Setting, Biota, Facies, and Evolution.; Permo-Carboniferous Carbonate Platforms and Reefs*, 78. Special Publication-Society for Sedimentary Geology.

Somerville, I. D. 2005. *Review of Irish Lower Carboniferous (Mississippian) Mud Mounds: Depositional Setting, Biota, Facies, and Evolution*, 83. AAPG Memoir.

Somerville, I. D. 2008. "Biostratigraphic Zonation and Correlation of Mississippian Rocks in Western Europe: Some Case Studies in the Late Viséan/Serpukhovian." *Geological Journal* 43, no. 2–3: 209–240. https://doi.org/10.1002/gj.1097.

Somerville, I. D., and A. R. E. Strank. 1984. "The Recognition of the Asbian/Brigantian Boundary Fauna and Marker Horizons in the Dinantian of North Wales." *Geological Journal* 19, no. 3: 227–237. https://doi.org/10.1002/gj.3350190303.

Somerville, I. D., A. R. E. Strank, and A. Welsh. 1989. "Chadian Faunas and Flora From Dyserth: Depositional Environments and Palaeogeographic Setting of Viséan Strata in Northeast Wales." *Geological Journal* 24, no. 1: 49–66. https://doi.org/10.1002/gj.3350240105.

Stuart, I. A., and G. Cowan. 1991. "The South Morecambe Field, Blocks 110/2a, 110/3a, 110/8a, UK East Irish Sea." *Geological Society Memoir* 14, no. 1: 527–541. https://doi.org/10.1144/GSL.MEM.1991.014.01.66.

Swennen, R., E. van der Voet, W. Wei, and P. Muchez. 2021. "Lower Carboniferous Fractured Carbonates of the Campine Basin (NE-Belgium) as Potential Geothermal Reservoir: Age and Origin of Open Carbonate Veins." *Geothermics* 96: 102147. https://doi.org/10.1016/j.geothermics.2021.102147.

Underhill, J. R., and N. Richardson. 2022. "Geological Controls on Petroleum Plays and Future Opportunities in the North Sea Rift Super Basin." *AAPG Bulletin* 106, no. 3: 573–631. https://doi.org/10.1306/07132120084.

van der Voet, E., B. Laenen, P. Muchez, et al. 2022. "Controls of Dolomitization and Bed Thickness on Fracture Networks in Lower Carboniferous Carbonates in Southern Belgium." *Journal of Structural Geology* 164: 104729. https://doi.org/10.1016/j.jsg.2022.104729.

Van Der Voet, E., B. Laenen, B. Rombaut, M. Kourta, and R. Swennen. 2020. "Fracture Characteristics of Lower Carboniferous Carbonates in Northern Belgium Based on FMI Log Analyses." *Netherlands Journal of Geosciences* 99: e8. https://doi.org/10.1017/njg.2020.6.

van Hulten, F. F. N. 2012. "Devono-Carboniferous Carbonate Platform Systems of The Netherlands." *Geologica Belgica* 15, no. 4: 284–296.

Van Tuyl, J., T. Alves, L. Cherns, G. Antonatos, P. Burgess, and I. Masiero. 2019. "Geomorphological Evidence of Carbonate Build-Up Demise on Equatorial Margins: A Case Study From Offshore Northwest Australia." *Marine and Petroleum Geology* 104: 125–149. https://doi.org/10.1016/j.marpetgeo.2019.03.006.

Van Tuyl, J., T. M. Alves, and L. Cherns. 2018. "Geometric and Depositional Responses of Carbonate Build-Ups to Miocene Sea Level and Regional Tectonics Offshore Northwest Australia." *Marine and Petroleum Geology* 94: 144–165. https://doi.org/10.1016/j.marpetgeo.2018.02.034.

Waters, C. N. 2009. "Carboniferous Geology of Northern England." *Journal of the Open University Geological Society* 30, no. 2: 5–16.

Waters, C. N. 2011. "A Revised Correlation of Carboniferous Rocks in the British Isles." In *A Revised Correlation of Carboniferous Rocks in the British Isles.* Geological Society of London. https://doi.org/10.1144/sr26.

Waters, C. N., R. B. Haslam, P. Cózar, I. D. Somerville, D. Millward, and M. Woods. 2017. "Mississippian Reef Development in the Cracoe Limestone Formation of the Southern Askrigg Block, North Yorkshire, UK." *Proceedings of the Yorkshire Geological Society* 61, no. 3: 179–196. https://doi.org/10.1144/pygs2016-374.

Weij, R., J. J. G. Reijmer, G. P. Eberli, and P. K. Swart. 2019. "The Limited Link Between Accommodation Space, Sediment Thickness, and Inner Platform Facies Distribution (Holocene–Pleistocene, Bahamas)." *Depositional Record* 5, no. 3: 400–420. https://doi.org/10.1002/dep2.50.

Worthington, R. P., and J. J. Walsh. 2011. "Structure of Lower Carboniferous Basins of NW Ireland, and Its Implications for Structural Inheritance and Cenozoic Faulting." *Journal of Structural Geology* 33, no. 8: 1285–1299. https://doi.org/10.1016/j.jsg.2011.05.001.

Wright, V. P. 1980. "Climatic Fluctuation in the Lower Carboniferous." *Naturwissenschaften* 67, no. 5: 252–253. https://doi.org/10.1007/BF01054535.

Wright, V. P., and S. D. Vanstone. 2001. "Onset of Late Palaeozoic Glacio-Eustasy and the Evolving Climates of Low Latitude Areas: A Synthesis of Current Understanding." *Journal of the Geological Society* 158, no. 4: 579–582. https://doi.org/10.1144/jgs.158.4.579.

Yaliz, A., and T. Chapman. 2003. "The Lennox Oil and Gas Field, Block 110/15, East Irish Sea." *Geological Society Memoir* 20, no. 1: 87–96. https://doi.org/10.1144/GSL.MEM.2003.020.01.07.

Zampetti, V., W. Schlager, J. H. van Konijnenburg, and A. J. Everts. 2004. "Architecture and Growth History of a Miocene Carbonate Platform From 3D Seismic Reflection Data; Luconia Province, Offshore Sarawak, Malaysia." *Marine and Petroleum Geology* 21, no. 5: 517–534. https://doi.org/10.1016/j.marpetgeo.2004.01.006.